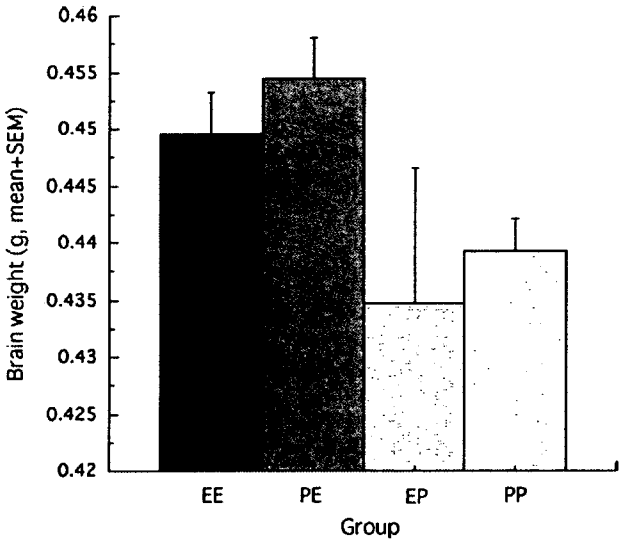

Fig. 6. Brain weight of four groups of mice. Brain was removed and weighted at the next day of the passive avoidance test (13 weeks old) (mean + S.E.M.).

Fig. 8 shows numbers of neurons stained for BrdU in hippocampus (A) and cerebral cortex (B). Neurons were counted in 10 sections for each animal, and were averaged. ANOVA including data for the hippocampus indicated the effect of group to be significant [$F(3, 24) = 8.516$, $p = .0005$]. Post hoc tests showed that group differences between EE and EP, EE and PP, EP and PE, and PE and PP were significant. Thus, environmental enrichment benefited generation of hippocampal neurons, with the most recent environment being critical. PE mice produced more new neurons in the hippocampus than EP mice. Next, ANOVA including data of the cerebral cortex also indicated that the effect of group was significant [$F(3, 25) = 3.169$, $p = .0418$]. Post hoc tests suggested that group differences between EE and EP, EP and PE, and EP and PP groups were significant.

Neurons thus began to increase significantly within 2 weeks after beginning of exposure to the enriched condition. Even a short period of enrichment augmented neuronal proliferation.

4. Discussion

Results of the present experiments reconfirmed that environmental enrichment between weaning and adult had affected development and function of the mouse brain. The brain was

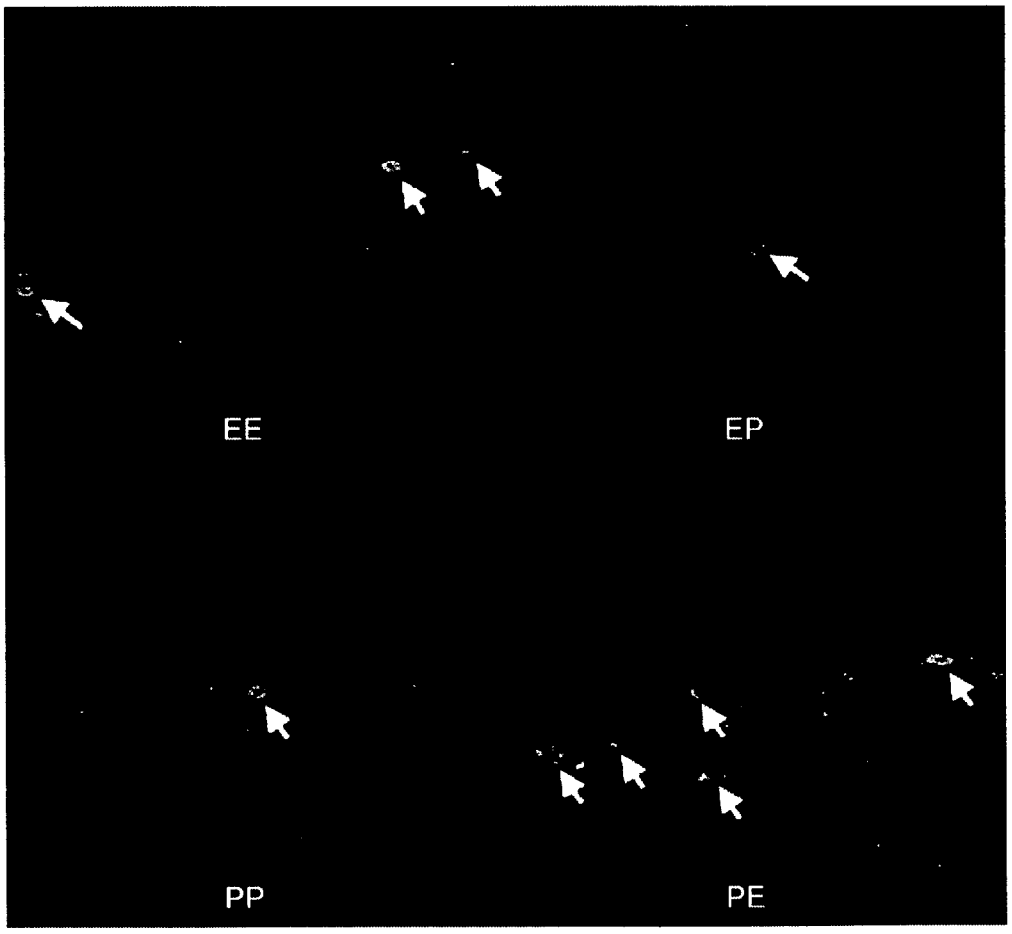

Fig. 7. Newly generated neurons in the hippocampus (arrows). Sections were visualized by confocal microscopy with antibody labeling for BrdU and PSA-NCAM. One example is presented for each group. Original magnification: 200×.

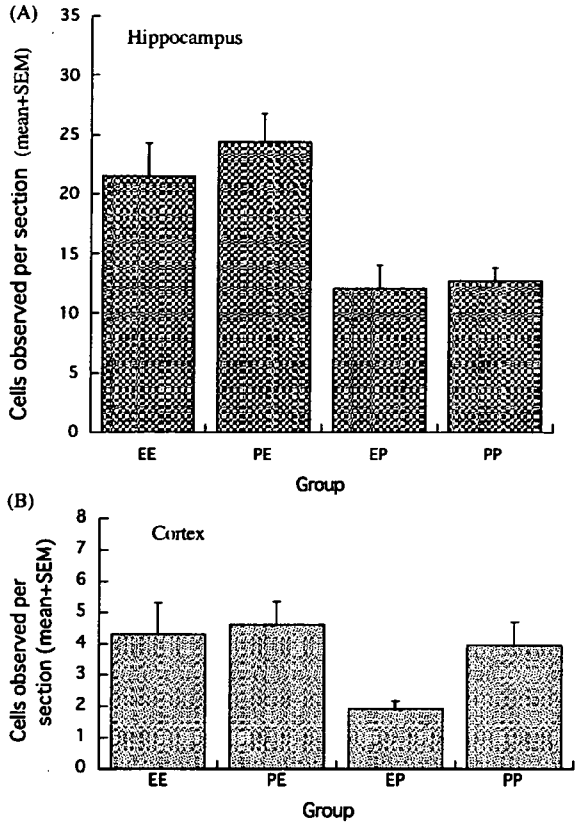

Fig. 8. Newly generated neurons in hippocampus (A) and cerebral cortex (B) per section (mean + S.E.M.). The two groups experienced enrichment during last 2 weeks (EE, PE) showed significantly more neurons labeled by BrdU than the two groups experienced impoverishment during last 2 weeks (EP, PP) in hippocampus. Group EP generated new neurons significantly less than the other three groups in cortex.

heavier in the EE group than the PP group, as in early studies [38,40]. Greater locomotive activities of the PP animals in the open-field test [10,33,41] and smaller prepulse inhibition in the PP mice than EE animals [6] were same as results reported in previous studies. Superior learning in EE mice compared with PP animals also agreed with results of earlier studies [11,29,50].

Moreover, results in the two environment exchange groups indicated that the effect of environment was determined by the most recent condition, suggesting that the plasticity or reorganisation of the brain could take place within a few weeks, even in adult mice. Behavioural results for PE mice resembled to the EE in open-field activity, startle amplitude, water-maze performance, and the probe test; brain weight also was greatest. Some researchers have reported that early impoverishment induced severe and irreversible deficiency in the rats' brain [9,13,51]. Or, development of the brain was not altered by impoverishment, once rats had experienced enrichment [19]. Our results of mice disagreed, the PE group, exposed to an impoverished environment in early life showed superior behavioural performance and heavier brains than the EP group exposed to an enriched environment during early life.

Indirect evidence has accumulated suggesting nervous tissue generation during enrichment [22,23,29,30], an effect also reported after running exercise [47,48]. We therefore expected that neurons would be generated during enriched experience in adult animals even over a short period. Indeed, long-term enrichment was found to increase hippocampal neurons in adult mice [20,21]. Our results in the PE and EP groups were critical in addressing this issue. The PE group generated many neurons in the hippocampus and cerebral cortex after a 2-week experience of enrichment, while results in the EP group suggested the beneficial effects of enrichment early in life could be nullified by impoverishment of conditions for 2 weeks, even in adult mice. Behavioural measures agreed with the anatomic data. PE mice performed better than EP animals, resembling the EE group. The present results that even a short period of enrichment promoted nerve cell generation with behavioural improvement, while a short period of impoverishment induced poor anatomic and behavioural outcomes, suggested that housing conditions are very important for reliable behavioural evaluation of experimental animals. Even "knockedout" mice missing a neurologically important gene reportedly recovered learning and memory after enrichment [8,35]. The results in this area of researches are almost always put in the context of enrichment [20,21,29,38–40]. However, the present results of the EP and PE groups suggest that it is important to study the effects of impoverishment as equally as enrichment. Standardization of housing conditions thus may be unexpectedly important in behavioural neuroscience.

We developed a speculative hypothesis concerning neuronal generation during enriched housing. After observing animals' behaviour in their home cages, enriched and impoverished animals lived completely differently. Enriched animals showed many types of movement, including running, chasing, crouching and fighting, hiding, climbing and wheel-running, and established social order among cage mates. These activities might activate neurons in specific areas of the brain such as hippocampus, cerebral cortex, hypothalamus, visual and motor areas and cerebellum. On the other hand, impoverished mice seldom moved, with less brain activation as a likely consequence. Activation of neurons could induce neurochemical excitation with an increase in regional cerebral blood flow as shown by functional magnetic resonance imaging (fMRI). Recent findings have shown neuronal regeneration after cerebral ischemia [3,28], regeneration was promoted if blood flow in ischemic brain was restored by angiogenesis [45]. Mechanisms underlying such effects are unclear, but recovery of blood flow might accelerate removal of debris or toxic products from the injured brain, and/or enhance production of chemokines and trophic agents [23,30]. If this hypothesis is true, neuron genesis and functional enhancement by enrichment in young adult mice might arise from brain stimulation and remodeling of blood flow. Our findings showed that an enriched environment enhanced neuron genesis in the mouse hippocampus and cingulated cortex, both of which participate in memory function. On the other hand, impoverished environment impaired neuron genesis. Based on these data, enriched experience appears to be essential for enhancing endogenous neuron genesis and improving functional recovery.

Recent animal welfare movement has advocated important of housing and care for laboratory rodents, giving animals greater

opportunity to carry out species-specific behavioural repertoires [4,18]. To answer the demand for standardized of environmental enrichment for laboratory animals, increasing numbers of rodent care products are coming available, even accommodating differences in preference for nest boxes in mice [46]. Improvements in housing conditions are expected to cause some discrepancies between early and present data, not only in behavioural observations but also for other biologic characteristics.

Finally, environmental enrichment has been used to promote the mental health of persons at risk [36,37]. For example, Rane et al. [36] assessed the effect of environmental enrichment including nutrition, education, and physical exercise at ages from 3 to 5 years in children with risk factors for later emergence of schizophrenia. Schizotypical personality features and antisocial behaviour were assessed at the ages of 17 and 23 years. Results suggested that the early enrichment program was effective; subjects who participated had more normal scores upon assessment in adolescence than untreated at-risk controls. These results are consistent with animal studies in which an enriched environment benefited behavioural and biologic outcomes. Moreover, our finding that even a short period of environmental enrichment positively affected behaviour and generation of neurons in the adult mouse suggested that even adults and elderly persons could benefit from enrichment, improving cognitive and memory functions. On the other hand, hospitalization or isolation might cause deterioration even in adults. Although the present experiment could not differentiate physical and social environments as the factor to influence the present results, we would like to testify whether social or physical, or the combination of both factors, cause the present effects in the future study.

Acknowledgments

This work was partially supported by a Grant-in Aid for Scientific Research (C) No. 17530540 in the Japanese Ministry of Education, Science, Sports and Culture and by a Research Grant for Cardiovascular Diseases. We would like to thank Ms. Yuka Okinaka for technical assistance.

References

[1] Akita H, Matsuyama T, Iso H, Sugita M, Yoshida S. Effects of oxidative stress on the expression of limbic-specific protease neuropsin and avoidance learning in mice. Brain Res 1997;967:86–96.
[2] Altman JA, Das GD. Autoradiographic examination of the effects of enriched environment on the rate of glial multiplication in the adult rat brain. Nature 1964:1161–3.
[3] Arvidsson A, Collin T, Kirik D, Kokaia Z, Lindvall O. Neuronal replacement from endogenous precursors in the adult brain after stroke. Nat Med 2002;8:963–70.
[4] Baumans V. Environmental enrichment for laboratory rodents and rabbits: requirements of rodents, rabbits, and research. ILAR J 2005;46:162–70.
[5] Benaroya-Milshtein N, Hollander N, Apter A, Kukulansky T, Raz N, Wilf A, et al. Environmental enrichment in mice decreases anxiety, attenuates stress responses and enhances natural killer cell activity. Eur J Neurosci 2004;20:1341–7.
[6] Cilia J, Reavill C, Hagan JJ, Jones DNC. Long-term evaluation of isolation-rearing induced prepulse inhibition deficits in rats. Psychopharmacology 2001;156:327–37.
[7] Dannis C. All in the mind of a mouse. Nature 2005;438:151–2.
[8] Duffy SN, Craddock KJ, Abel T, Nguyen PV. Environmental enrichment modifies the PKA-dependence of hippocampal LTP and improves hippocampus-dependent memory. Learn Memory 2001;8:26–34.
[9] Einon DF, Morgan MJ. A critical period for social isolation in the rat. Dev Psychobiol 1977;10:123–32.
[10] Elliott BM, Grunberg NE. Effects of social and physical enrichment on open field activity differ in male and female Sprague–Dawley rats. Behav Brain Res 2005;165:187–96.
[11] Ferchmin PA, Eterovic VA. Forty minutes of experience increase the weight and RNA content of cerebral cortex in periadolescent rats. Dev Psychobiol 1986;19:511–9.
[12] Ferchmin PA, Eterovic VA, Caputto R. Studies of brain weight and RNA content after short periods of exposure to environmental complexity. Brain Res 1970;20:49–57.
[13] File SE. Exploration, distraction, and habituation in rats reared in isolation. Dev Psychobiol 1978;11:73–81.
[14] Gentch C, Lichtsteiner M, Frischnecht HR, Feer H, Siegfried B. Isolation-induced locomotor hyper-activity and hypoanalgesia in rats are prevented by handling and reversed by resocialisation. Physiol Behav 1988;43:13–6.
[15] Gobbo OL, O'Mara SM. Impact of enriched-environment housing on brain-derived neurotrophic factor and on cognitive performance after a transient global ischemia. Behav Brain Res 2004;152:231–41.
[16] Gottleb G, Blair C. How early experience matters in intellectual development in the case of poverty. Prevent Sci 2004;5:245–52.
[17] Huck UW, Price EO. Differential effects of environmental enrichment on the open-field behavior of wild and domestic Norway rats. J Comp Physiol Psychol 1975;89:892–8.
[18] Hutchinson E, Avery A, Vandewoude S. Environmental enrichment for laboratory rodents. ILAR J 2005;46:148–61.
[19] Katz HB, Davies CA. Effects of differential environments on the cerebral anatomy of rats as a function of previous and subsequent housing conditions. Exp Neurol 1984;83:274–87.
[20] Kempermann G, Brandon EP, Gage FH. Environmental stimulation of 129/SvJ mice causes increased cell proliferation and neurogenesis in the adult dentate gyrus. Curr Biol 1998.
[21] Kempermann G, Kuhn HG, Gage FH. More hippocampal neurons in adult mice living in an enriched environment. Nature 1997;386:493–5.
[22] Leggio MG, Mandolesi L, Federico F, Spirito F, Ricci B, Gelfo F, et al. Environmental enrichment promotes improved spatial abilities and enhanced dendritic growth in the rat. Behav Brain Res 2005;163:78–90.
[23] Lewis MH. Environmental complexity and central nervous system development and function. Mental Retard Dev Disabil Rev 2004;10:91–5.
[24] Lodge DJ, Lawrence AJ. The effect of isolation rearing on volitional ethanol consumption and central CCK/dopamine systems in Fawn-Hooded rats. Behav Brain Res 2003;141:113–22.
[25] Matsuyama S, Doe N, Kurihara N, Tanizawa K, Kuroda S, Iso H, et al. Spatial learning of mice lacking a neuron-specific epidermal growth factor family protein, NELL2. J Pharmacol Sci 2005;98:239–43.
[26] McIlwain KL, Merriweather MY, Yuva-Paylor LA, Paylor R. The use of behavioral test batteries: effects of training history. Physiol Behav 2001;73:705–17.
[27] Morgan MJ. Effects of post-weaning environment on learning in the rat. Anim Behav 1973;21:429–42.
[28] Nakatomi H, Kuriu T, Okabe S, Yamamoto S, Hatano O, Kawahara N, et al. Regeneration of hippocampal pyramidal neurons after ischemic brain injury by recruitment of endogenous neural progenitors. Cell 2002;110:429–41.
[29] Pham TM, Soderstrom S, Winblad B, Mohammed AH. Effects of environmental enrichment on cognitive function and hippocampal NGF in the non-handled rats. Behav Brain Res 1999;103:63–70.
[30] Pham TM, Winblad B, Granholm A, Mohammed AH. Environmental influences on brain neurotrophines in rats. Pharmacol Biochem Behav 2002;73:167–75.
[31] Phillips GD, Howes SR, Whitelaw RB, Robbins TW, Everitt BJ. Isolation rearing impairs the reinforcing efficacy of intravenous cocaine or intra-accumbens D-amphetamine: impaired response to intra-accumbens D1 and D2/D3 dopamine receptor antagonists. Psychopharmacology 1994;115:419–29.

[32] Phillips GD, Howes SR, Whitelaw RB, Wilkinson LS, Robbins TW, Everitt BJ. Isolation rearing enhances the locomotor response to cocaine and a novel environment, but impairs the intravenous self-administration of cocaine. Psychopharmacology 1994;115:407–18.
[33] Pietropaolo S, Branchi I, Cirulli F, Chiarotti F, Aloe L, Alleva E. Long-term effects of the periadolescent environment on exploratory activity and aggressive behaviour in mice: social versus physical enrichment. Physiol Behav 2004;81:443–53.
[34] Pryce CR, Bettschen D, Nanz-Bahr NI, Feldon J. Comparison of the effects of early handling and early deprivation on conditioned stimulus, context, and spatial learning and memory in adult rats. Behav Neurosci 2003;117:883–93.
[35] Rampon C, Tang Ya-P, Goodhouse J, Shimizu E, Kyin M, Tsien JZ. Enrichment induces structural changes and recovery from nonspatial memory deficit in CA1 NMDAR1-knockout mice. Nat Neurosci 2000;3:238–45.
[36] Rane A, Mellingen K, Liu J, Vanables PH, Mednick SA. Effects of environmental enrichment at ages 3–5 years on schizotypical personality and antisocial behavior at ages 17 and 23 years. Am J Psychiatry 2003;160:1627–35.
[37] Rane A, Vanables PH, Dalais C, Mellingen K, Reynolds C, Mednick SA. Early educational and health enrichment at age 3–5 years is associated with increased autonomic and central nervous system arousal and orienting at age 11 years: evidence from Mauritius Child Health Project. Psychophysiology 2001;38:254–66.
[38] Rosenzweig MR. Environmental complexity, cerebral change, and behavior. Am Psychol 1966;21:321–32.
[39] Rosenzweig MR, Bennett EL. Psychobiology of plasticity: effects of training and experience on brain and behavior. Behav Brain Res 1996;78:57–65.
[40] Rosenzweig MR, Krech D, Bennett EL, Diamond MC. Effects of environmental complexity and training on brain chemistry and anatomy: a replication and extension. J Comp Physiol Psychol 1962;55:429–37.
[41] Sahakian BJ, Robbins TW, Morgan MJ, Iversen SD. The effects of psychomotor stimulants on stereotypy and locomotor activity in socially-deprived and control rats. Brain Res 1975;84:195–205.
[42] Sasaki H, Iso H, Coffey P, Inoue T, Fukuda Y. Prepulse facilitation of auditory startle response in hamsters. Neurosci Lett 1998;248:117–20.
[43] Seki T, Arai Y. The persistent expression of a highly polysialylated NCAM in the dentate gyrus of the adult rat. Neurosci Res 1991;12:503–13.
[44] Seki T, Arai Y. Highly polysialylated neural cell adhesion molecule (NCAM) is expressed by newly generated granule cells in the dentate gyrus of the adult rat. J Neurosci 1993;13:2351–8.
[45] Taguchi A, Soma T, Tanaka H, Kanda T, Nishimura H, Yoshikawa H, et al. Administration of CD34+ cells after stroke enhances neurogenesis via angiogenesis in a mouse model. J Clin Invest 2004;114:330–8.
[46] Van Loo PL, Bloom HJ, Meijer MK, Baumans V. Assessment of the use of two commercially available environmental enrichments by laboratory mice by preference testing. Lab Anim 2005;39:58–67.
[47] Van Praag H, Cristie BR, Sejnowski TJ, Gage FH. Running enhances neurogenesis, learning and long-term potentiation in mice. Proc Natl Acad Sci USA 1999;96:13427–31.
[48] Van Praag H, Kempermann G, Gage FH. Running increases cell proliferation and neurogenesis in the adult mouse dentate gyrus. Nat Neurosci 1999;2:266–70.
[49] Van Praag H, Kempermann G, Gage FH. Neural consequences of environmental enrichment. Nat Rev Neurosci 2000;1:191–8.
[50] Wood WE, Greenough WT. Effect of grouping and crowding on learning in isolation-reared adult rats. Bull Psychon Soc 1974;3:65–7.
[51] Wright IK, Upton N, Marsden CA. Resocialization of isolation-reared rats does not alter their anxiogenic profile on the elevated X-maze model of anxiety. Physiol Behav 1991;50:1129–32.
[52] Yukawa K, Iso H, Tanaka T, Tsubota Y, Owada-Makabe K, Bai T, et al. Down-regulation of dopamine transporter and abnormal behavior in STAT6-deficient mice. Int J Mol Med 2005;15:819–25.
[53] Yukawa K, Tanaka T, Owada-Makabe K, Tsubota Y, Bai T, Maeda M, et al. Reduced prepulse inhibition of startle in STAT6-deficient mice. Int J Mol Med 2005;16:673–5.

ORIGINAL RESEARCH

Visualization of Intracerebral Arteries by Synchrotron Radiation Microangiography

K. Myojin
A. Taguchi
K. Umetani
K. Fukushima
N. Nishiura
T. Matsuyama
H. Kimura
D.M. Stern
Y. Imai
H. Mori

BACKGROUND AND PURPOSE: Small cerebral vessels are a major site for vascular pathology leading to cerebral infarction and hemorrhage. However, such small cerebral vessels are difficult to visualize by using conventional methods. The goal of our study was the development of methodology allowing visualization of small cerebral arteries in rodents, suitable for experimental models.

MATERIALS AND METHODS: Using barium sulfate as a contrast material, we obtained microangiographic images of physiologic and pathologic changes consequent to cerebral infarction in mouse brain by monochromatic synchrotron radiation (SR). To achieve high-resolution and high-contrast images, we used a new x-ray camera with a pixel size of 4.5 μm, and we set the energy level at 37.5 keV, just above the K absorption of barium.

RESULTS: Small intracerebral arteries (~30 μm in diameter) were clearly visualized, as well as the cortical branches (50–70 μm in diameter) at the brain surface. The limit of detection appeared to be vessels ~10 μm in diameter. Compared with the noninfarcted side, the number of intracerebral arteries was dramatically decreased in the middle cerebral artery area affected by stroke.

CONCLUSIONS: These results indicate the potential of SR for evaluating pathologic changes in small cerebral arteries and for monitoring the impact of pro- and antiangiogenic therapeutic strategies.

Cerebrovascular disease is one of the major causes of death and disability in developed countries. To evaluate cerebral vasculature, conventional angiography and MR angiography are commonly used in clinical practice. The development of these imaging methods has allowed analysis of the pathologic features of cerebrovascular lesions and has guided therapeutic strategies. However, small cerebral vessels, including those known to harbor causative lesions in cerebral infarction and hemorrhage (due to lipohyalinotic changes and/or microaneurysm formation),[1] such as intracerebral arteries and perforators, are below the detection limit of conventional imaging techniques. An important step in developing therapeutic strategies effective against disease in small cerebral vessels is enhanced visualization of this vasculature, especially in experimental models.

Recently, ex vivo and in vivo microangiography using monochromatic synchrotron radiation (SR) has been suggested as a tool capable of visualizing pathophysiologic changes in small arteries. Using this system has made possible the detection of microcirculation in the dermis,[2] tumors,[3] and collateral microvessels in ischemic hind limbs.[4] Although fluorescence microscopy has also been used to image small arteries,[5-7] SR imaging has the advantage of visualizing microvessels, even after they enter the parenchyma of an organ. In contrast, fluorescence techniques do not allow adequate visualization of small arteries once a vessel is deep within brain or other parenchymal tissue. On the basis of these observations, we have developed a microangiographic system using SR and have investigated physiologic and pathologic features of rodent cerebral microvasculature.

Received August 3, 2006; accepted after revision August 31.

From the Departments of Cerebrovascular Disease (K.M., A.T.) and Cardiac Physiology (K.F., N.N., H.M.), National Cardiovascular Center, Osaka, Japan; the Department of Radiology (K.M., Y.I.), Tokai University School of Medicine, Kanagawa, Japan; Japan Synchrotron Radiation Research Institute (K.U.), Hyogo, Japan; the Department of Internal Medicine (T.M.), Hyogo College of Medicine, Hyogo, Japan; Dainippon Sumitomo Pharma Co Ltd (H.K.), Osaka, Japan; and the Dean's Office (D.M.S.), College of Medicine, Cincinnati University, Cincinnati, Ohio.

Experiments were performed at the SPring-8 BL28B2 beamline with the approval of the Japan Synchrotron Radiation Research Institute (acceptance No. 2005B0358).

This work was partially supported by a Grant-in-Aid for Scientific Research from the Ministry of Health, Labor and Welfare and The New Energy and Industrial Technology Development Organization.

Please address correspondence to Akihiko Taguchi, MD, Department of Cerebrovascular Disease, National Cardiovascular Center, 5-7-1 Fujishiro-dai, Suita, Osaka, Japan, 565-8565; e-mail: Taguchi ataguchi@res.ncvc.go.jp

Materials and Methods

All procedures were performed in accordance with the National Cardiovascular Center Animal Care and Use Committee.

Preparation of Contrast Medium

For high-contrast images of the microcirculation, contrast agents included microspheres (Techpolymer I-2, Sekisui Plastics, Shiga, Japan) and barium sulfate (BarytgenSol, Fushimi, Tokushima, Japan). However, because the diameter of microspheres was 15 μm, whereas that of barium sulfate particles varied from 1–100 μm, the microcirculation of cerebral arteries could not be visualized by using these contrast media (not shown). To perfuse such microvessels (diameter <10 μm), we filtered barium sulfate (pore size 5 μm; Millex-SV, Millipore, Bedford, Mass) and obtained particles <5 μm in diameter. Filtered barium sulfate particles were then centrifuged (3000 G, 60 minutes) and concentrated to 50% by weight following removal of the supernatant.

Injection of Contrast Medium

Male severe combined immunodeficient (SCID) mice (6 weeks old; weight, 25–30 g; Oriental Yeast, Tokyo, Japan) were anesthetized by using inhaled diethyl ether and were perfused systemically with phosphate-buffered saline (PBS) containing heparin (40 U/mL) via the left ventricle of the heart with a peristaltic pump (Iwaki, Asahi Techno Glass, Chiba, Japan). Filtered barium sulfate particles (<5 μm in diameter, prepared as described previously; 50% by weight) were infused (0.7 mL), followed by isolation of the brain and fixation in formalin.

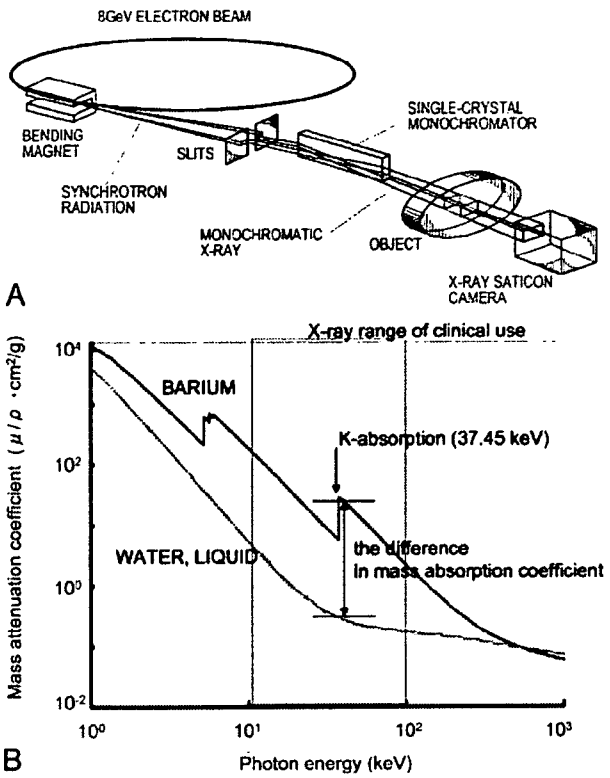

Fig 1. Schematic depiction of the monochromatic SR system. *A*, Illustration of the experimental arrangement for SR microangiography at BL28B2. *B*, Photon mass attenuation coefficient of barium (*blue line*) and liquid water (*red line*). Monochromatic x-ray energy is adjusted to 37.5 keV, just above the barium K-edge energy to produce the highest contrast image.

Microangiography and Image Analysis

Microangiographic images of mouse brain were obtained by using monochromatic SR in the Japan Synchrotron Radiation Research Institute (SPring-8, Hyogo, Japan).[4,8] There are 3 large 3rd-generation synchrotron radiation facilities in the world: the Advanced Photon Source in Argonne (United States), the European Synchrotron Radiation Facility in Grenoble (France), and SPring-8 (the latter was used for the studies described herein). These facilities are open to scientists in many fields, including material, chemical, and life sciences investigators. The experimental setup for x-ray imaging by using monochromatic SR at the SPring-8 BL28B2 beamline is shown in Fig 1*A*. The storage ring was operated at 8-GeV electron beam energy, and beam current was 80–100 mA. The distance between the point source in the bending magnet and the detector was ~45 m. A nearly parallel x-ray beam was used for imaging without blurring because of the small size of the x-ray source and the very long source-to-object distance. The single crystal monochromator selects a single energy of synchrotron radiation. The shutter system is located between the monochromator and the object. X-rays transmitted through the object are detected by an x-ray direct-conversion-type detector incorporating the x-ray saticon pickup tube. Monochromatic x-ray energy was adjusted to 37.5 keV, just above the barium K-edge energy, to produce the highest contrast image of the barium (Fig 1*B*). X-ray flux at the object position was around 1×10^{10} photons/mm^2 per second in imaging experiments. The images were acquired as 1024 × 1024 pixels with 10-bit resolution after analog-to-digital conversion. The FOV was 4.5 × 4.5 mm^2, and pixel size was ~4.5 μm.[9,10]

Mammographic Images

To compare spatial and contrast resolution, we obtained mammographic images, which are known for having the highest resolution in clinical applications,[11] of murine brains. Digital images were captured at an energy level of 24 kV by using a molybdenum target and a molybdenum filter with 90° cranial projection. Source-to-image distance was 65 cm.

Induction of Focal Cerebral Ischemia

Permanent focal cerebral infarction was induced by ligation and disconnection of the left MCA of male SCID mice (n = 5), as described.[12–14] Briefly, under inhaled halothane (3%) anesthesia, animals were placed on their right sides and a skin incision was made at the midpoint between the left orbit and the external auditory canal. The temporalis muscle was incised, and the zygomatic arch was removed to expose the squamous portion of the temporal bone. Using a dental drill, we made a small hole above the distal portion, M1, of the MCA, which could be seen through the exposure in the skull. The dura mater was opened, and the left MCA was electrocauterized and disconnected just distal to its crossing of the olfactory tract. Body temperature was maintained at 36.5°–37°C by using a heat lamp during the operation and for 2 hours after MCA occlusion. Cerebral blood flow (CBF) in the left MCA area was measured by laser-Doppler flowmetry (Advance, Tokyo, Japan). The holding device of the laser probe (ALF probe; Neuroscience, Osaka, Japan) (1.5 mm in diameter, 7.0 mm in length) was secured on the cranium at a site located above the ischemic core of the left MCA area (approximately 1 mm anterior and 5 mm distal to the bregma), and CBF was monitored during the procedure and 24 hours after ligation of the MCA. Mice displaying a decrease in CBF by ~75% immediately after the procedure and thereafter for an additional 24 hours were used for experiments.[15] Nine days after induction of cerebral ischemia, the cerebral microcirculation was examined by SR imaging.

MR Imaging System

To confirm cerebral infarction consequent to ligation of the MCA, we performed MR imaging on day 2 poststroke. MR imaging used a 2T compact MR imaging system with a permanent magnet (MRmini SA206, Dainippon Sumitomo Pharma, Osaka, Japan) by using a radio-frequency solenoid coil for signal-intensity detection. For each imaging sequence, 15 coronal images were acquired with a section thickness of 1 mm, gapped at 0.5 mm. T1-weighted spin-echo MR images were acquired with a TR/TE of 500/9 ms, a FOV of 36.6 × 18.3 mm, an image acquisition matrix of 256 × 128, and NEX, 4. T2-weighted spin-echo MR images were obtained with TR/TE, 3000/69, 256 × 128, and NEX, 2. Because the sequences to obtain diffusion-weighted images by using this machine are still in development, we evaluated the cerebral ischemia by T2-weighted images on day 2 poststroke.

Data Analysis

In all experiments, the mean ± SE is reported.

Results

Visualization of Cerebral Arteries by SR Imaging

After euthanasia and systemic perfusion with PBS, barium sulfate particles were infused via the left ventricle of the heart. As shown in Fig 2*A*, cerebral arteries on the brain surface were filled with contrast medium. First, we investigated vascular

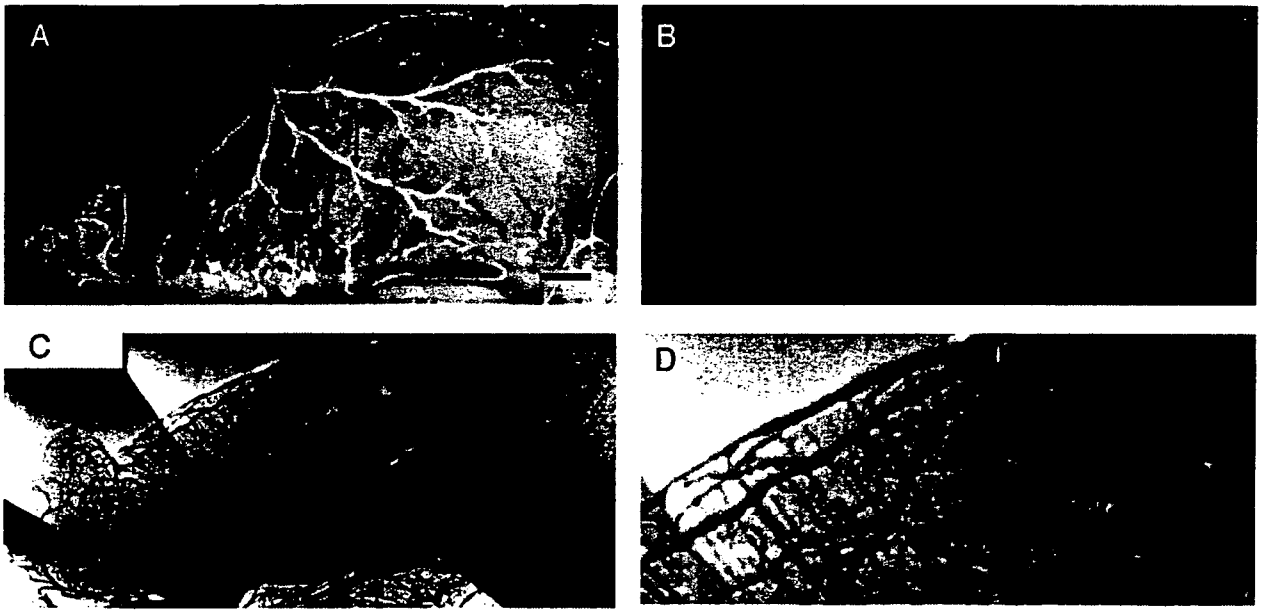

Fig 2. Angiographic image of mouse cerebral artery. *A*, Macroimage of the right brain hemisphere. The cerebral arteries (*arrows*), but not cerebral veins, are filled with the barium sulfate. *B*, Cerebral microangiogram (90° caudal projection) with a mammographic soft x-ray machine. Mammography enables visualization of small cerebral arteries and penetrating intracerebral arteries, but the image is not sufficient to evaluate pathologic changes. *C* and *D*, Cerebral angiograms obtained by SR. Note that small cerebral vessels, including penetrating intracerebral arteries, are clearly visualized. Microvascular structures, such as orthogonal branching of penetrating intracerebral arteries from the cortical artery, are clearly observed by the enlarged SR imaging (*D*). *E*, Coronal section of a cerebral microangiogram. Two distinct penetrating intracerebral arteries, superficial penetrating arteries and deep penetrating arteries (*arrow*), are clearly observed by the SR image. Scale bars: 1 mm (*A* and *B*), 0.5 mm (*C* and *E*), and 250 μm (*D*).

images by mammography (Fig 2*B*). However, sufficient spatial and contrast resolution was not obtained by mammographic imaging to evaluate the angioarchitecture of small cerebral vasculature. Peripheral branches of the MCA (75–100 μm in diameter) and small vessels emerging from peripheral branches were barely visualized.

Next, we investigated the vascular profile by using SR (Fig 2*C*, normal view; -*D*, enlarged view). At the brain surface, cortical arteries branching from the MCA and pial arteries, ~30 μm in diameter, were clearly visualized. Within the brain parenchyma, penetrating intracerebral arteries, branching orthogonally from cortical or pial arteries, were also observed. The interval between intracerebral arteries was 126.1 ± 35.5 μm (n = 20), the diameter of the proximal side of the intracerebral arteries was 29.5 ± 3.1 μm (n = 20), and each intracerebral artery was observed to progressively narrow to a diameter below the limit of resolution (10 μm). Vascular diameters determined by SR imaging of intracerebral arteries and small arterial branches were identical to those observed in previous pathologic studies of murine brain.[16] Using SR imaging, we could discern 2 types of intracerebral arteries: superficial penetrating arteries perfusing only the cortical area and penetrating arteries reaching the subcortical area and perfusing the deep white matter. These vascular structures observed in murine brain by SR imaging are similar to previous observations in human anatomic studies.[17-20] Compared with mammographic images, SR imaging enabled visualization of penetrating intracerebral arteries (diameter range of 10–30 μm), as well as small peripheral branches of MCA at the brain surface, with remarkable clarity. Using a coronal view for cerebral microangiograms, we also discerned 2 distinct penetrating arteries, superficial and deep (Fig 2*E*).

SR Images after Cerebral Infarction

To evaluate cerebral vasculature in the context of pathologic changes, cerebral infarction was induced by ligation of the MCA. The area of cerebral infarction was visualized by MR imaging on day 2 after induction of stroke. As we have shown previously by 2,3,5-triphenyltetrazolium staining,[12] limited cortical infarction was observed in the MCA area on T2-weighted images (Fig 3*A*). In contrast, no hyper- or hypointense region was observed on T1-weighted images (Fig 3*B*), indicating the absence of bleeding or parenchymal injury. Although no morphologic (Fig 3*C*) or vascular structural (Fig 3*D*) changes were observed in the right hemisphere (nonstroke side), by day 9 after MCA occlusion, tissue degradative changes were observed in the cortical and shallow white matter of the left MCA area (stroke side, Fig 3*E*). To evaluate the integrity of the microvasculature after stroke, we obtained SR images. The number of penetrating intracerebral arteries dramatically decreased, though cortical branches at the brain surface could still be visualized (Fig 3*F*). On the coronal view, the disappearance of the intracerebral arteries on the ischemic side was also clearly observed (Fig 3*G*).

Discussion

Cerebral artery disease in small vessels is a major cause of cerebral infarction and hemorrhage. Although pathologic changes in small arteries have been reported on the basis of microscopic analysis, it has been difficult to assess the mor-

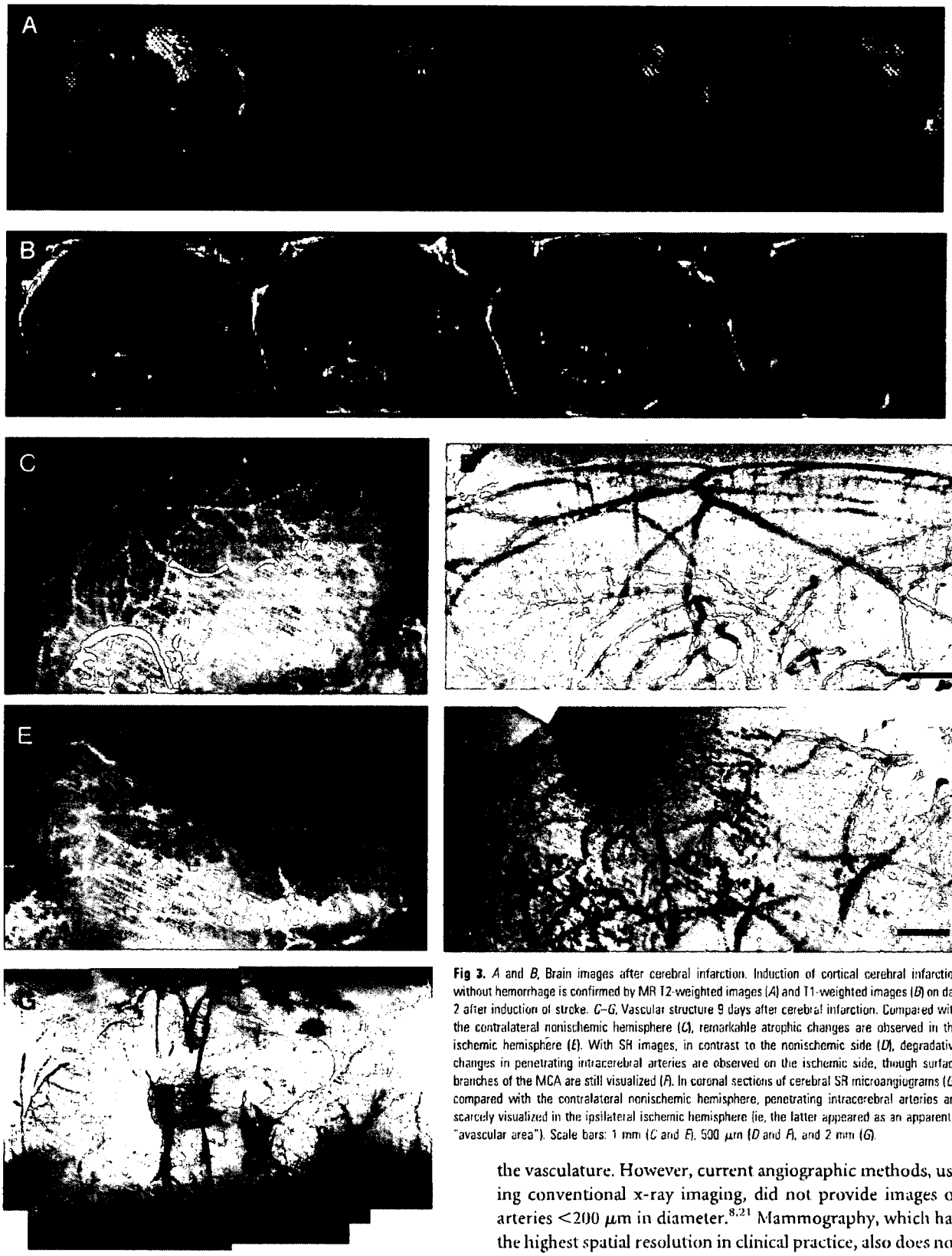

Fig 3. *A* and *B*, Brain images after cerebral infarction. Induction of cortical cerebral infarction without hemorrhage is confirmed by MR T2-weighted images (*A*) and T1-weighted images (*B*) on day 2 after induction of stroke. *C–G*, Vascular structure 9 days after cerebral infarction. Compared with the contralateral nonischemic hemisphere (*C*), remarkable atrophic changes are observed in the ischemic hemisphere (*E*). With SR images, in contrast to the nonischemic side (*D*), degradative changes in penetrating intracerebral arteries are observed on the ischemic side, though surface branches of the MCA are still visualized (*F*). In coronal sections of cerebral SR microangiograms (*G*), compared with the contralateral nonischemic hemisphere, penetrating intracerebral arteries are scarcely visualized in the ipsilateral ischemic hemisphere (ie, the latter appeared as an apparently "avascular area"). Scale bars: 1 mm (*C* and *E*), 500 μm (*D* and *F*), and 2 mm (*G*).

phology of small cerebral vessels in situ through imaging studies. Herein, we demonstrate that small cerebral vessels can be clearly visualized by microangiography by using SR.

Conventional angiography is commonly used to evaluate the vasculature. However, current angiographic methods, using conventional x-ray imaging, did not provide images of arteries <200 μm in diameter.[8,21] Mammography, which has the highest spatial resolution in clinical practice, also does not have sufficient resolution to visualize small vessels with a diameter of <50 μm.[11] Microangiographic techniques have been developed by using fine-focus x-rays and sensitive films to evaluate the microcirculation in the brain.[20] These methods enable visualization of human cortical perforating arteries and

medullary long branches (100 μm in diameter) by using 1-cm-thick sections of brain.[20] However, the limit of detection by using these methods applied to thick sections has been reported to be vessels of 50 μm in diameter.[22] Furthermore, visualization of smaller arteries required thin sections cut with a microtome.[20] The latter method is not well-suited to the evaluation of 3D cerebral vascular trees.

Compared with these conventional methods, the principal advantage of SR is the small size of the electron beam, thereby providing a high-intensity x-ray point source. Using a nearly parallel beam of SR, along with a precise detection system (pixel size of 4.5 μm), allowed us to obtain high-quality angiographic images with excellent spatial resolution. Furthermore, setting SR at an energy level just above the K absorption of barium produced the highest contrast images. SR imaging provides a powerful tool to reveal the morphology of small cerebral arteries such as superficial and deep penetrating arteries, allowing analysis of their physiologic and pathologic properties under a variety of conditions (ie, borderzone in infarction[23,24] and microaneurysm formation).

Fluorescence microscopy is another tool potentially useful for analysis of the microcirculation.[25] Although fluorescence microscopy provides visualization of microcirculation at the brain surface, the advantage of SR imaging is visualization of small vessels that have penetrated into the brain parenchyma, such as the subcortex. In addition, SR imaging allows performance of microangiography with an optimal projection. When the latter is combined with a microinjector, sequential real-time images can be obtained, providing the substrate for hemodynamic analysis.

In this article, we investigated SR imaging after stroke and showed that the SR image reflects pathologic changes previously observed by using anatomic/microscopic analysis. On day 9 after MCA occlusion, arteries on the surface of the cerebrum were visualized by SR, though penetrating intracerebral arteries were not detected. Previous studies have shown that the integrity of the distal cortical artery is usually maintained after occlusion of the proximal artery and that collateral flow is established through expansion of previously existing and/or formation of new vascular channels.[25,26] Analysis with enhanced MR imaging has shown cerebral parenchymal enhancement in the stroke area by 1 week after cerebral infarction,[27] indicative of blood flow in the peri-ischemic area. In contrast, penetrating intracerebral arteries were dramatically decreased in number in the ischemic hemisphere, though cortical branches on the brain surface were maintained after MCA occlusion. It has previously been shown that microvasculature in the ischemic territory displays adhesion of polymorphonuclear leukocytes in postcapillary venules, followed by the disruption of the microvascular network.[28] These previous findings are consistent with the results of our vascular images obtained by SR after ligation of the MCA.

Conclusion

Our study demonstrates, for the first time, the morphologic features of small vascular networks in murine brain by microangiography by using SR imaging. Our approach provides a powerful tool for evaluating potential angiogenic/antiangiogenic therapeutic strategies, as well as pathologic examination of the cerebral microarterial tree.

Acknowledgments

We thank Y. Kasahara, K. Tomiyasu, and M. Aoki for technical assistance.

References

1. Phillips SJ, Whisnant JP. **Hypertension and the brain: The National High Blood Pressure Education Program.** *Arch Intern Med* 1992;152:938–45
2. Ito K, Tanaka E, Mori H, et al. **A microangiographic technique using synchrotron radiation to visualize dermal circulation in vivo.** *Plast Reconstr Surg* 1998;102:1128–33
3. Tokiya R, Umetani K, Imai S, et al. **Observation of microvasculatures in athymic nude rat transplanted tumor using synchrotron radiation microangiography system.** *Academic Radiology* 2004;9:1039–46
4. Takeshita S, Isshiki T, Mori H, et al. **Use of synchrotron radiation microangiography to assess development of small collateral arteries in a rat model of hindlimb ischemia.** *Circulation* 1997;95:805–08
5. Conway JG, Popp JA, Thurman RG. **Microcirculation in periportal and pericentral regions of lobule in perfused rat liver.** *Am J Physiol* 1985;249:G349–56
6. Stock RJ, Cilento EV, McCuskey RS. **A quantitative study of fluorescein isothiocyanate-dextran transport in the microcirculation of the isolated perfused rat liver.** *Hepatology* 1989;9:75–82
7. Birngruber R, Schmidt-Erfurth U, Teschner S, et al. **Confocal laser scanning fluorescence topography: a new method for three-dimensional functional imaging of vascular structures.** *Graefes Arch Clin Exp Ophthalmol* 2000;238:559–65
8. Mori H, Hyodo K, Tanaka E, et al. **Small-vessel radiography in situ with monochromatic synchrotron radiation.** *Radiology* 1996;201:173–77
9. Umetani K, Yagi N, Suzuki Y, et al. **Observation and analysis of microcirculation using high-spatial-resolution image detectors and synchrotron radiation.** *Proceeding of SPIE* 2000;3977:522–33
10. Yamashita T, Kawashima S, Ozaki M, et al. **Images in cardiovascular medicine: mouse coronary angiograph using synchrotron radiation microangiography.** *Circulation* 2002;105:E3–4
11. Kuzmiak CM, Pisano ED, Cole EB, et al. **Comparison of full-field digital mammography to screen-film mammography with respect to contrast and spatial resolution in tissue equivalent breast phantoms.** *Med Phys* 2005;32:3144–50
12. Taguchi A, Soma T, Tanaka H, et al. **Administration of CD34+ cells after stroke enhances neurogenesis via angiogenesis in a mouse model.** *J Clin Invest* 2004;114:330–38
13. Furuya K, Kawahara N, Kawai K, et al. **Proximal occlusion of the middle cerebral artery in C57Black6 mice: relationship of patency of the posterior communicating artery, infarct evolution, and animal survival.** *J Neurosurg* 2004;100:97–105
14. Kitagawa K, Matsumoto M, Mabuchi T, et al. **Deficiency of intercellular adhesion molecule 1 attenuates microcirculatory disturbance and infarction size in focal cerebral ischemia.** *J Cereb Blood Flow Metab* 1998;18:1336–45
15. Matsushita K, Matsuyama T, Nishimura H, et al. **Marked, sustained expression of a novel 150-kDa oxygen-regulated stress protein, in severely ischemic mouse neurons.** *Brain Res Mol Brain Res* 1998;60:98–106
16. Coyne EF, Ngai AC, Meno JR, et al. **Methods for isolation and characterization of intracerebral arterioles in the C57/BL6 wild-type mouse.** *J Neurosci Methods* 2002;120:145–53
17. Herman LH, Ostrowski AZ, Gurdjian ES. **Perforating branches of the middle cerebral artery: an anatomical study.** *Arch Neurol* 1963;8:32–34
18. Kaplan HA. **The lateral perforating branches of the anterior and middle cerebral arteries.** *J Neurosurg* 1965;23:305–10
19. de Reuck J. **The area of the deep perforating branches of the median cerebral artery in man** [in French]. *Acta Anat (Basel)* 1969;74:30–35
20. Salamon G, Combalbert A, Faure J, et al. **Microradiographic study of the arterial circulation of the brain.** *Prog Brain Res* 1968;30:33–41
21. Mori H, Hyodo K, Tubita K, et al. **Visualization of penetrating transmural arteries in situ by monochromatic synchrotron radiation.** *Circulation* 1994;89:863–71
22. Salamon G, Raybaud C, Michotey P, et al. **Angiographic study of cerebral convolutions and their area of vascularization** [in French]. *Rev Neurol (Paris)* 1975;131:259–84
23. Bogousslavsky J, Regli F. **Centrum ovale infarcts: subcortical infarction in the superficial territory of the middle cerebral artery.** *Neurology* 1992;42:1992–98
24. Donnan GA, Norrving B, Bamford JM, et al. **Subcortical infarctions: classification and terminology.** *Cerebrovasc Dis* 1993;3:248–51
25. Tomita Y, Kubis N, Calando Y, et al. **Long-term in vivo investigation of mouse cerebral microcirculation by fluorescence confocal microscopy in the area of focal ischemia.** *J Cereb Blood Flow Metab* 2005;25:858–67
26. Zulch KJ. *Cerebral Circulation and Stroke*. Berlin, Germany: Springer-Verlag; 1971:116
27. Merten CL, Knitelius HO, Assheuer J, et al. **MRI of acute cerebral infarcts: increased contrast enhancement with continuous infusion of gadolinium.** *Neuroradiology* 1999;41:242–48
28. del Zoppo GJ, Mabuchi T. **Cerebral microvessel responses to focal ischemia.** *J Cereb Blood Flow Metab* 2003;23:879–94

European Journal of Neuroscience, Vol. 26, pp. 126–133, 2007 doi:10.1111/j.1460-9568.2007.05640.x

Granulocyte colony-stimulating factor has a negative effect on stroke outcome in a murine model

Akihiko Taguchi,[1] Zhongmin Wen,[1] Kazunori Myojin,[1] Tomoyuki Yoshihara,[1] Takayuki Nakagomi,[2] Daisuke Nakayama,[1] Hidekazu Tanaka,[3] Toshihiro Soma,[4] David M. Stern,[5] Hiroaki Naritomi[1] and Tomohiro Matsuyama[2]

[1]Department of Cerebrovascular Disease, National Cardiovascular Center, 5-7-1 Fujishiro-dai, Suita, Osaka, Japan, 565-8565
[2]Department of Advanced Medicine, Hyogo College of Medicine, Hyogo, Japan
[3]Department of Pharmacology, Graduate School of Medicine, Osaka University, Osaka, Japan
[4]Department of Hematology, Osaka Minami National Hospital, Osaka, Japan
[5]Dean's Office, College of Medicine, University of Cincinnati, OH, USA

Keywords: angiogenesis, cerebral infarction, inflammation, neuroprotection

Abstract

The administration of CD34-positive cells after stroke has been shown to have a beneficial effect on functional recovery by accelerating angiogenesis and neurogenesis in rodent models. Granulocyte colony-stimulating factor (G-CSF) is known to mobilize CD34-positive cells from bone marrow and has displayed neuroprotective properties after transient ischemic stress. This led us to investigate the effects of G-CSF administration after stroke in mouse. We utilized permanent ligation of the M1 distal portion of the left middle cerebral artery to develop a reproducible focal cerebral ischemia model in CB-17 mice. Animals treated with G-CSF displayed cortical atrophy and impaired behavioral function compared with controls. The negative effect of G-CSF on outcome was associated with G-CSF induction of an exaggerated inflammatory response, based on infiltration of the peri-infarction area with CD11b-positive and F4/80-positive cells. Although clinical trials with G-CSF have been started for the treatment of myocardial and limb ischemia, our results indicate that caution should be exercised in applying these results to cerebral ischemia.

Introduction

Granulocyte colony-stimulating factor (G-CSF) was identified in 1975 and has been broadly used for mobilizing granulocytes from bone marrow (Weaver *et al.*, 1993). G-CSF is also known to mobilize immature hematopoietic cells that include endothelial progenitor cells (EPCs) (Willing *et al.*, 2003). In view of the capacity of circulating EPCs to enhance neovascularization of ischemic tissues (Asahara *et al.*, 1997), the results of recent studies demonstrating that infusion of EPCs accelerates angiogenesis at ischemic sites, thereby limiting tissue injury, is not unexpected (Dzau *et al.*, 2005). As a potential extension of this concept, administration of G-CSF has been shown to accelerate angiogenesis in animal models of limb and myocardial ischemia (Minatoguchi *et al.*, 2004). These observations have provided a foundation for clinical trials testing the effects of G-CSF in limb and myocardial ischemia (Kuethe *et al.*, 2004).

Stroke, a critical ischemic disorder in which there are important opportunities for neuroprotective therapies, is another situation in which enhanced angiogenesis might be expected to improve outcome. For example, we have shown that the administration of CD34-positive cells after stroke accelerates angiogenesis and, subsequently, neurogenesis (Taguchi *et al.*, 2004). Similarly, erythropoietin (EPO), also known to have angiogenic properties, has been shown to have beneficial effects in experimental cerebral ischemia (Ehrenreich *et al.*, 2002; Wang *et al.*, 2004). In addition, G-CSF displays neuroprotective properties *in vitro* (Schabitz *et al.*, 2003) and *in vivo* (Schabitz *et al.*, 2003; Shyu *et al.*, 2004; Gibson *et al.*, 2005), the latter in a rodent model of transient cerebral ischemic damage. Models of transient cerebral ischemia allow subtle assessment of neuroprotective properties, such as the survival of vulnerable neuronal populations in the penumbra. However, functional outcome after stroke is also determined by inflammation and reparative processes consequent to extensive brain necrosis, the latter better modelled by permanent cerebral ischemia. We have evaluated the effect of G-CSF on stroke outcome in a model of permanent cerebral ischemia with massive cell necrosis. Our model employs permanent ligation of the left middle cerebral artery (MCA) and results in extensive neuronal death in the ischemic zone, as well as more selective apoptotic cell death in the penumbral area (Walther *et al.*, 2002). Using this model, we have tested the effect of G-CSF on functional recovery after stroke.

Materials and methods

All procedures were performed under the auspices of an approved protocol of the Japanese National Cardiovascular Center Animal Care and Use Committees (protocol no. 06026, approval date, May 22, 2006).

Induction of focal cerebral ischemia

To assess the effect of G-CSF on stroke, we developed a highly reproducible murine stroke model applying our previous method

Correspondence: Dr Akihiko Taguchi, as above.
E-mail: ataguchi@res.ncvc.go.jp

Received 19 October 2006, revised 25 April 2007, accepted 21 May 2007

(Taguchi *et al.*, 2004) to CB-17 mice (Clea, Tokyo, Japan). Under halothane anesthesia (inhalation of 3%), the left zygoma was dissected to visualize the MCA through the cranial bone. A hole was made using a dental drill in the bone (diameter 1.5 mm) and the MCA was carefully isolated, electro-cauterized and disconnected just distal to its crossing of the olfactory tract (distal M1 portion). Cerebral blood flow in the MCA area was monitored as described previously (Matsushita *et al.*, 1998). Briefly, an acrylate column was attached to the intact skull using stereotactic coordinates (1 mm anterior and 3 mm lateral to the bregma) and cerebral blood flow was assessed using a linear probe (1 mm in diameter) by laser Doppler flowmetry (Neuroscience Co. Ltd, Osaka, Japan). Mice that showed decreased cerebral blood flow by ~75% immediately after the procedure were used for experiments (success rate of > 95%). Body temperature was maintained at 36.5–37 °C using a heat lamp (Nipponkoden, Tokyo, Japan) during the operation and for 2 h after MCA occlusion. At later timepoints, mice were first subjected to behavioral tests and then to histological examination of their brains. For histological examination, mice were perfusion-fixed with 100 mL of periodate-lysine-paraformaldehyde fixative under deep (pentobarbital) anesthesia (100 mg/kg, intraperitonealy) and their brains were removed. Coronal brain sections (20 μm) were cut on a vibratome (Leica, Solms, Germany) and subjected to immunocytochemistry.

Administration of granulocyte colony-stimulating factor and erythropoietin following stroke

To examine the effect of G-CSF on ischemic cerebral injury, human recombinant G-CSF (Kirin, Tokyo, Japan) was administered subcutaneously at four doses (0.5, 5, 50 or 250 μg/kg) at 24, 48 and 72 h after induction of stroke. As controls, the same volume of phosphate-buffered saline (PBS) or recombinant human EPO (1000 μg/kg; Kirin), the latter known to have angiogenic properties and a positive effect on stroke outcome (Jaquet *et al.*, 2002), was administered subcutaneously. Other time courses of G-CSF administration, including 1 h after stroke (at doses of 0.5, 5, 50 or 250 μg/kg) and continuous administration (100 μg/kg/day) by micro-osmotic pump (Durect, Cupertino, CA, USA) started 1 h after stroke over 7 days, were also studied. To exclude possible effects of an immune response to human recombinant G-CSF in the mouse, murine recombinant G-CSF (R & D Systems, Minneapolis, MN, USA; doses of 0.5, 5 or 50 μg/kg) was administered subcutaneously at 24, 48 and 72 h after induction of stroke, as indicated.

Immunohistochemistry

To evaluate the inflammatory response following administration of G-CSF post-stroke, brain sections were studied immunohistochemically using antibody to CD11b (BD Biosciences, San Jose, CA, USA) and F4/80 (Serotec, Raleigh, NC, USA). The numbers of CD11b-positive inflammatory cells at the anterior cerebral artery (ACA)/MCA border of the infarcted area and numbers of F4/80-positive ($F4/80^+$) activated microglia/macrophages in the ACA area at the exact center of the forebrain section (at the midpoint of the left forebrain, as shown with an orange line in Fig. 1J) were scored by two investigators blinded to the experimental protocol.

Analysis of the peri-infarction and infarcted area after middle cerebral artery occlusion

To investigate mechanisms of brain damage/atrophy consequent to administration of G-CSF, neovessel formation and the extent of infarction were analysed. Formation of new vessels was assessed at the border of the MCA and ACA territories by perfusing carbon black (0.5 mL; Fuekinori, Osaka, Japan) via the left ventricle of the heart. Staining with 2,3,5-triphenyltetrazolium (TTC) (Sigma-Aldrich, St Louis, MO, USA) was employed to demarcate the border of viable/non-viable tissue. Semiquantitative analysis of angiogenesis employed an angiographic score. Briefly, microscopic digital images were scanned into a computer (Keyence, Osaka, Japan) and the number of carbon black-positive microvessels crossing the border zone of the TTC-negative MCA area to the TTC-positive ACA area was determined. To evaluate the infarcted area 3 days after stroke, coronal brain sections at the exact center of the forebrain were stained with TTC. The infarcted area was measured using a microscopic digital camera system (Olympus, Tokyo, Japan). Infarction in this stroke model was highly reproducible and limited to the left cortex. NIH IMAGE software was used to quantify the TTC-positive area in the ACA territory. A brain atrophy index was established using whole brain images captured by a digital camera system (Olympus). The length of the forebrain was measured along the x and y dimensions shown in Fig. 1J and the ratio of $x : y$ was defined as the brain atrophy index.

Behavioral analysis

To assess cortical function, mice were subjected to behavioral testing using the open field task (Kimble, 1968) at 35 days after stroke. In this behavioral paradigm, animals were allowed to search freely in a square acrylic box (30 × 30 cm) for 60 min. A light source on the ceiling of the enclosure was on during the first 30 min (light period) and was turned off during a subsequent 30-min period. On the X- and Y-banks of the open field, two infrared beams were mounted 2 cm above the floor, spaced at 10 cm intervals, forming a flip–flop circuit between them. The total number of beam crossings by the animal was counted and scored as traveling behavior (locomotion). Twelve infrared beams were set 5 cm above the floor, spaced at 3 cm intervals, on the X-bank and the total number of beam crossings was counted and scored as rearing behavior (rearing). To exclude the contribution of physical deficits directly related to the operative procedure and induction of stroke, motor deficiencies were examined on day 35 after stroke. Neurological deficits were scored on a three-point modified scale as described previously (Tamatani *et al.*, 2001): 0, no neurological deficit; 1, failure to extend the left forepaw fully; 2, circling to left and 3, loss of walking or righting reflex. Body weight, monitored in each experimental group, displayed no significant differences (data not shown).

Data analysis

Statistical comparisons among groups were determined using one-way ANOVA and the Dunnett test was used for post-hoc analysis to compare with PBS controls. Where indicated, individual comparisons were performed using Student's t-test. In all experiments, mean ± SEM is reported.

Results

Induction of stroke in CB-17 mice

In a previous report, we demonstrated reproducible strokes in severe combined immunodeficient (SCID) mice by permanent ligation of the left MCA (Taguchi *et al.*, 2004). As SCID mice originated from the CB-17 strain, we expected anatomical similarity of cerebral arteries in

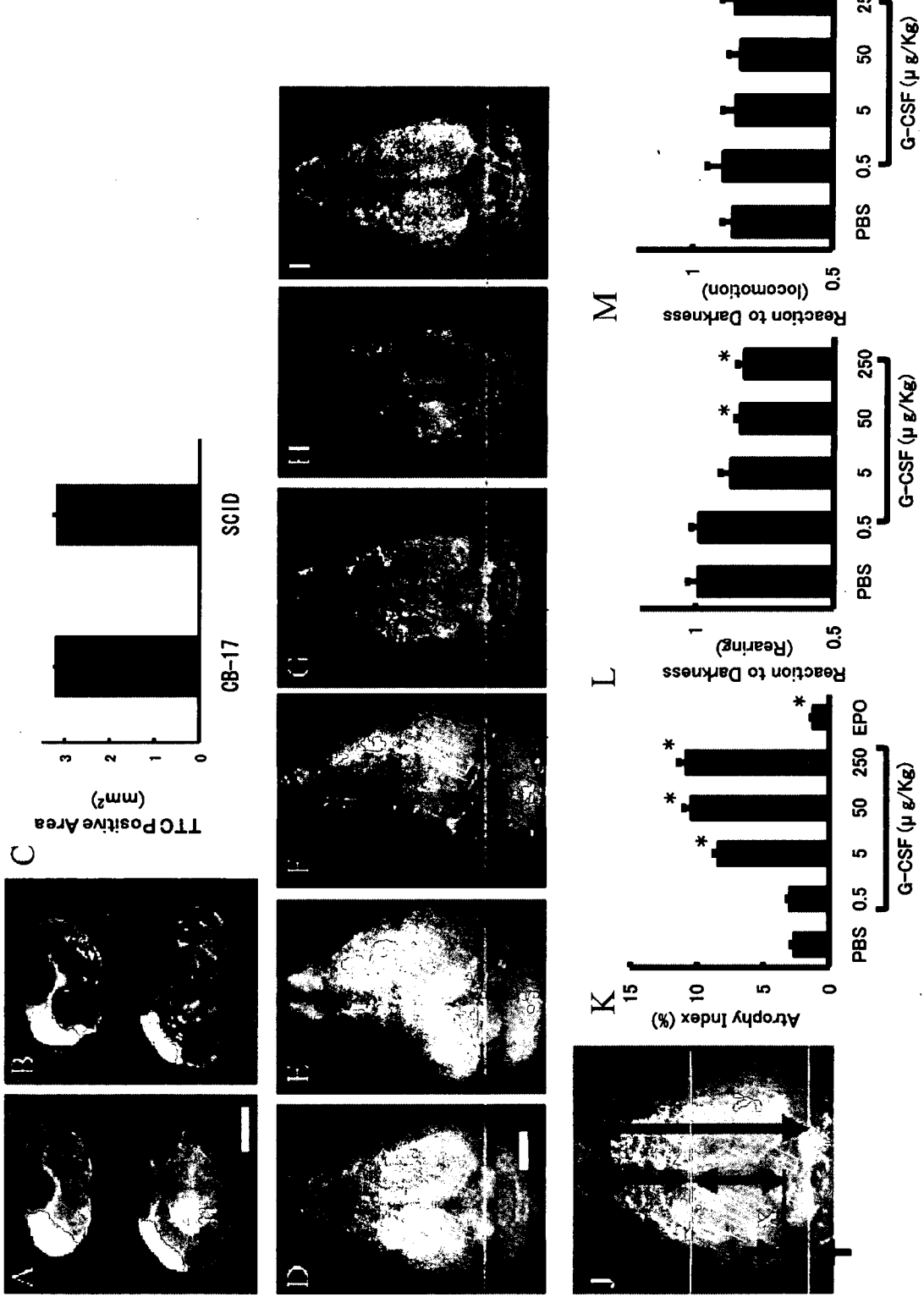

FIG. 1. Administration of granulocyte colony-stimulating factor (G-CSF) induces cortical atrophy. (A–C) Induction of stroke by ligation of the M1 portion of the left middle cerebral artery (MCA). Forebrain sections harvested from mice 3 h after stroke were stained with 2,3,5-triphenyltetrazolium (TTC), and lack of positive staining is observed in the MCA cortex of CB-17 (A) and severe combined immunodeficient (SCID) mice (B). The TTC-positive anterior cerebral artery area at the exact center of forebrain was quantified using NIH IMAGE (C). A highly reproducible TTC-positive (surviving) cortical area was observed in CB-17 and SCID mice. (D–I) On day 35 post-stroke, brains were evaluated grossly. Compared with post-stroke mice treated with phosphate-buffered saline (PBS) (D), no significant difference was observed in mice treated with 0.5 μg/kg of G-CSF (E). In contrast, brain atrophy was observed with G-CSF treatment at doses of 5 μg/kg (F), 50 μg/kg (G) or 250 μg/kg (H). Treatment with erythropoietin (EPO) (I) had a beneficial effect in terms of brain atrophy. Note that, compared with the contralateral side (green line), atrophy in the longitudinal direction was observed in animals treated with G-CSF (F–H). (J) A brain atrophy index was defined as the ratio of $x : y$. (K) ANOVA analysis ($n = 6$ per group) revealed significant brain atrophy in mice at doses of G-CSF above 0.5 μg/kg. In contrast, a reduction of brain atrophy was observed in mice treated with EPO. (L and M) Behavioral analysis post-stroke. ANOVA analysis ($n = 6$ per group) in mice subjected to stroke revealed that treatment with either 50 or 250 μg/kg of G-CSF significantly impaired the rearing response compared with PBS (L), although no significant difference was observed in locomotion (M). Marker bars, 2 mm (A and D). $^*P < 0.05$ *vs.* PBS.

these two strains. Strokes were induced in CB-17 mice by permanent ligation of the M1 distal portion of the left MCA. To evaluate the infarcted area, brain sections were stained with TTC at 3 h after stroke. Reproducible strokes were induced in CB-17 mice (Fig. 1A) that were similar to those in SCID mice (Fig. 1B). The surviving cortical area post-stroke, represented by the TTC-positive ACA area at the exact center of forebrain, was also similar in CB-17 and SCID mice (Fig. 1C, $n = 6$/species).

Granulocyte colony-stimulating factor accelerates brain injury after stroke

In a previous study, we demonstrated that enhanced neovascularization post-stroke, due to administration of CD34-positive cells, promoted neuronal regeneration leading to cortical expansion and functional recovery (Taguchi *et al.*, 2004). As G-CSF is known to mobilize CD34-positive cells from bone marrow (Kuethe *et al.*, 2004), we investigated the effects of G-CSF treatment, starting 24 h after stroke and continuing for 3 days, using the above permanent focal cerebral ischemia model. Compared with control animals receiving PBS alone (Fig. 1D), no significant difference was observed in mice that received 0.5 μg/kg of G-CSF (Fig. 1E and K) at 35 days after stroke. However, remarkable brain atrophy was observed with G-CSF treatment at 5 μg/kg (Fig. 1F and K), 50 μg/kg (Fig. 1G and K) or 250 μg/kg (Fig. 1H and K). In contrast, a mild protective effect, with respect to brain atrophy, was observed in the group treated with EPO post-stroke (1000 μg/kg; Fig. 1I and K). In each condition depicted in Fig. 1, a representative image is shown and quantitative analysis of the brain atrophy index ($n = 6$/experimental condition; defined in Fig. 1J) is demonstrated in Fig. 1K.

Granulocyte colony-stimulating factor has a negative effect on functional recovery after stroke

To investigate functional recovery in animals treated with G-CSF, we performed behavioral testing on day 35 after stroke ($n = 6$, for each group). Compared with post-stroke CB-17 mice that received PBS, mice treated with 50 or 250 μg/kg G-CSF displayed impaired behavioral function as assessed by the 'dark' response, with respect to rearing (Fig. 1L and Table 1) analysed by ANOVA followed by post-hoc Dunnett test, although there was no significant change in locomotion (Fig. 1M). In contrast, treatment with EPO accelerated functional recovery with respect to both rearing (1.18 ± 0.07 and 0.99 ± 0.04 in EPO and PBS groups, respectively, $n = 6$ per group, $P < 0.05$) and locomotion (1.04 ± 0.04 and 0.85 ± 0.04 in EPO and PBS groups, respectively, $n = 6$ per group, $P < 0.05$). Mice showed rapid recovery from focal motor deficits and, by day 16 post-stroke, no motor deficits were detected based on a modified three-point scale (not shown).

Granulocyte colony-stimulating factor accelerates angiogenesis after stroke

Increased brain atrophy and impaired functional recovery in animals treated with G-CSF post-stroke were quite unexpected because of the known ability of G-CSF to mobilize CD34-positive cells from bone marrow (Willing *et al.*, 2003). In addition, a previous study showed neuroprotective properties of G-CSF in models of transient cerebral ischemia (Schabitz *et al.*, 2003). These considerations led us to analyse mechanisms contributing to increased brain atrophy after

TABLE 1. Raw data of open field test (G-CSF rearing)

Treatment and individual	Rearing (counts)		Reaction to darkness (Right OFF/Right ON)
	Right ON	Right OFF	
PBS			
1	662	640	0.97
2	611	708	1.16
3	487	450	0.92
4	587	540	0.92
5	482	430	0.89
6	425	450	1.06
Mean ± SEM	542.3 ± 37.2	536.3 ± 47.1	0.99 ± 0.04
G-CSF (0.5μg/kg)			
1	600	562	0.94
2	601	650	1.08
3	494	425	0.86
4	731	731	1.00
5	767	784	1.02
6	498	501	1.01
Mean ± SEM	615.2 ± 46.7	608.8 ± 56.2	0.98 ± 0.03
G-CSF (5μg/kg)			
1	577	497	0.86
2	537	368	0.69
3	310	288	0.93
4	520	485	0.93
5	673	652	0.97
6	572	480	0.84
Mean ± SEM	531.5 ± 49.3	461.7 ± 50.8	0.87 ± 0.04
G-CSF (50μg/kg)			
1	592	520	0.88
2	463	376	0.81
3	478	430	0.90
4	307	250	0.81
5	484	410	0.85
6	385	295	0.77
Mean ± SEM	451.5 ± 39.6	380.2 ± 39.6	0.84 ± 0.02
G-CSF (250μg/kg)			
	578	424	0.73
	501	401	0.80
	507	380	0.75
	465	412	0.89
	380	341	0.90
	401	347	0.87
Mean ± SEM	472 ± 29.9	384.2 ± 14.0	0.82 ± 0.03

Right ON, under light condition; Right OFF, under dark condition.

administration of G-CSF. As G-CSF has been reported to accelerate angiogenesis in limb and cardiac models of ischemic injury (Minatoguchi *et al.*, 2004), we sought to determine its impact on neovascularization in our permanent focal cerebral infarction model. Compared with PBS-treated controls (Fig. 2A), increased neovasculature at the border of the MCA and ACA cortex (staining with TTC demarcates viable/non-viable tissue and carbon black was used to visualize vessels) was observed in animals treated with G-CSF (50 μg/kg, Fig. 2B). Assessment of the angiographic score confirmed the impression of increased neovasculature in animals treated with G-CSF, compared with the group receiving PBS (Fig. 2C; $P < 0.05$).

Next, we investigated possible neuroprotective properties of G-CSF after stroke. Analysis of the infarcted/surviving area 3 days after stroke was evaluated in animals treated with PBS (Fig. 2D) or G-CSF (50 μg/kg, Fig. 2E) based on TTC staining; there was no effect of G-CSF treatment compared with controls receiving PBS (Fig. 2F). Thus, G-CSF did not impact on the viability of 'at-risk' tissue in the

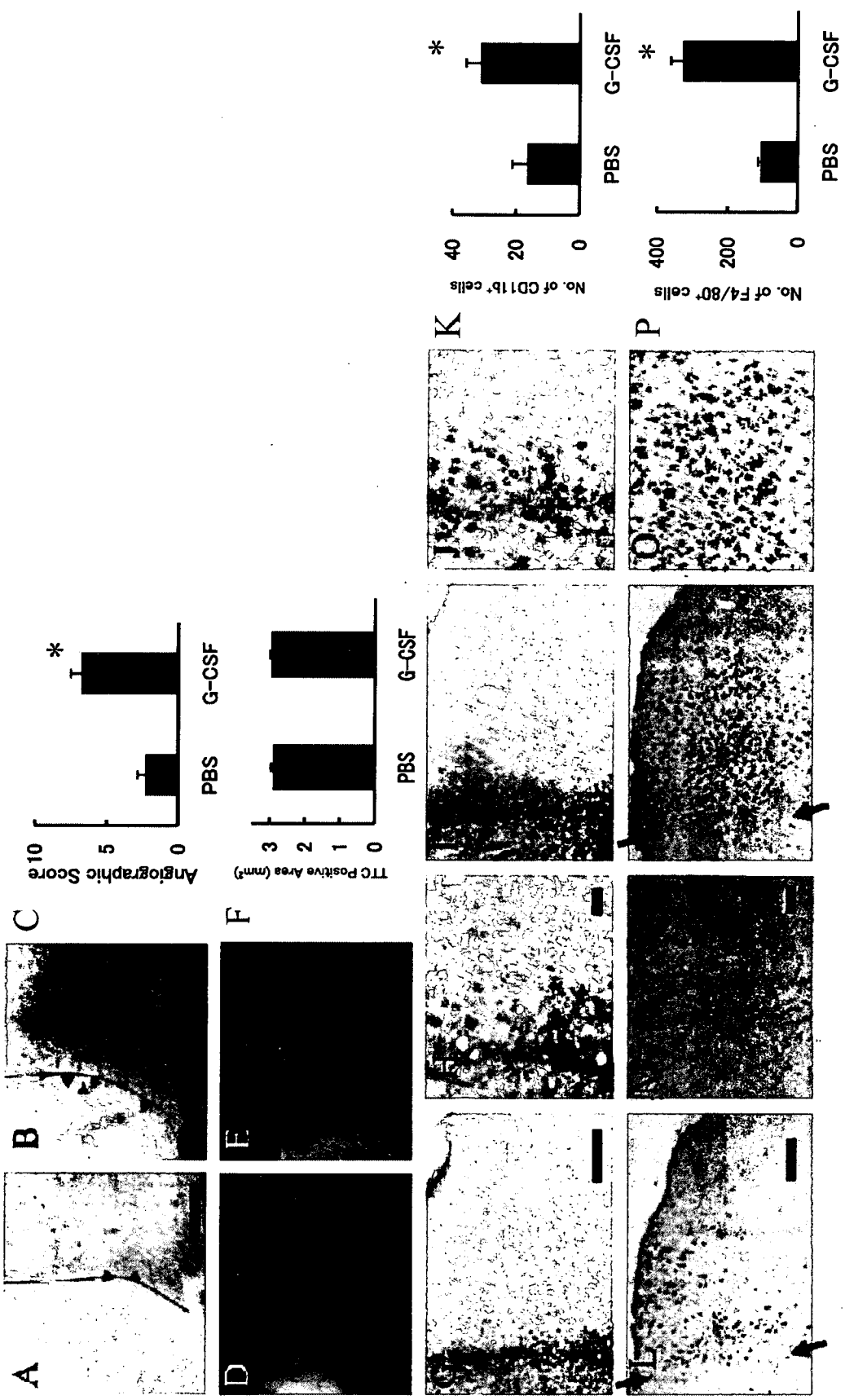

FIG. 2. Administration of granulocyte colony-stimulating factor (G-CSF) after stroke enhances the inflammatory response. (A–C) On day 3 after stroke, mice were infused with carbon black ink. Compared with mice treated with phosphate-buffered saline (PBS) (A), increased neovascularization was observed at the border between anterior cerebral artery (ACA) and middle cerebral artery (MCA) regions in mice treated with G-CSF (B). Representative micrographs are shown. The angiographic score (see Materials and methods) showed increased neovascularization ($n = 6$ per group) in mice treated with G-CSF post-stroke compared with controls (PBS). (D–F) There was no difference in the 2,3,5-triphenyltetrazolium (TTC)-positive ACA area at the exact center of forebrain comparing post-stroke animals treated with G-CSF (E) and controls/PBS (D). Sections from each animal were subjected to statistical analysis using Student's *t*-test ($n = 6$ animals per group; F). (G–K) CD11b-positive cells were visualized in the ACA area in tissue from post-stroke animals treated with PBS (G, lower magnification; H, higher magnification) or G-CSF (I, lower magnification; J, higher magnification). Sections from each animal were evaluated ($n = 6$ animals per group) and the average number of CD11b-positive cells per high power field is shown in each of the two groups (K). (L–P) F4/80-positive ($F4/80^+$) activated macrophages/microglia in mice treated with PBS were relatively limited to the area close to the border of infarcted tissue (L, lower magnification; M, higher magnification). However, an expanded area and increased density of $F4/80^+$ cells was observed after administration of G-CSF (N, lower magnification; O, higher magnification). The total number of $F4/80^+$ activated macrophages/microglia in the viable ACA area identified on the section at exact center of forebrain was quantified ($n = 6$ per group) (N). Scale bars: 0.2 mm (A), 1 mm (D), 0.3 mm (G and L) and 30 μm (H and M). $^*P < 0.05$ vs. PBS. Arrowheads (A and B) indicate microvessels at the border of the MCA and ACA cortex (red line). Arrows (L and N) indicate the border of infarcted tissue (left side, stroke MCA area; right side, viable ACA area).

immediate post-stroke period (up to 3 days), although there was a long-term effect on brain atrophy (evaluated at 35 days).

Granulocyte colony-stimulating factor enhances the inflammatory response after stroke

Further studies were performed to analyse the apparent dichotomy between G-CSF-mediated enhancement of neovascularization of the ischemic territory post-stroke vs. increased cerebral atrophy and lack of improvement in behavioral testing. We focused our studies on the inflammatory response. Compared with PBS-treated mice (Fig. 2G, lower magnification; Fig. 2H, higher magnification), increased accumulation of CD11b-positive inflammatory cells, including monocytes and granulocytes (Campanella *et al.*, 2002), was observed in G-CSF-treated mice (50 μg/kg) at the border of the infarcted area (Fig. 2I, lower magnification; Fig. 2J, higher magnification). Quantitative analysis ($n = 6$ each) revealed a significant difference in the number of infiltrating CD-11b-positive cells (Fig. 2K; $P < 0.05$). These results led us to evaluate the presence of activated macrophages/microglia in ischemic lesions, as the latter are known to enhance brain damage after stroke (Mabuchi *et al.*, 2000). Although F4/80$^+$ activated macrophages/microglia were observed in the viable (i.e. non-ischemic) ACA area following treatment with PBS (Fig. 2L, lower magnification; Fig. 2M, higher magnification), increased numbers of F4/80$^+$ macrophages/microglia were observed in post-stroke animals treated with G-CSF (Fig. 2N, lower magnification; Fig. 2O, higher magnification). F4/80$^+$ activated macrophages/microglia in post-stroke mice treated with PBS were principally limited to the area close to the border of the infarcted tissue. In contrast, F4/80$^+$ cells in post-stroke mice treated with G-CSF were observed in a broad area and at higher density in the ACA territory. The total number of F4/80$^+$ cells in a section at the exact center of the forebrain was quantified ($n = 6$ each); a significant increase in F4/80$^+$ activated macrophages/microglia was observed in G-CSF-treated mice, compared with controls receiving PBS post-stroke (Fig. 2P; $P < 0.05$).

Administration of granulocyte colony-stimulating factor 1 h after stroke also induces brain atrophy

As the experimental protocol for the above studies involved G-CSF treatment starting 24 h after stroke, it was important to vary our protocol. For this purpose, we also administered G-CSF within 1 h of stroke (Fig. 3A, $n = 6$ each) or performed continuous treatment for up to 7 days (Fig. 3B, $n = 6$ each). Our results demonstrate induction of brain atrophy in post-stroke animals treated with G-CSF subjected to either of these protocols compared with PBS-treated controls.

To exclude the immune response stimulated by human recombinant G-CSF in mice, various doses of mouse recombinant G-CSF were administered and the effect was determined ($n = 6$ each dose). We found significant brain atrophy with administration of lower doses (0.5 and 5 μg/kg) of recombinant murine G-CSF. As the survival rate was only 50% (three mice dead out of six) with administration of a higher dose (50 μg/kg), the group was excluded from this analysis.

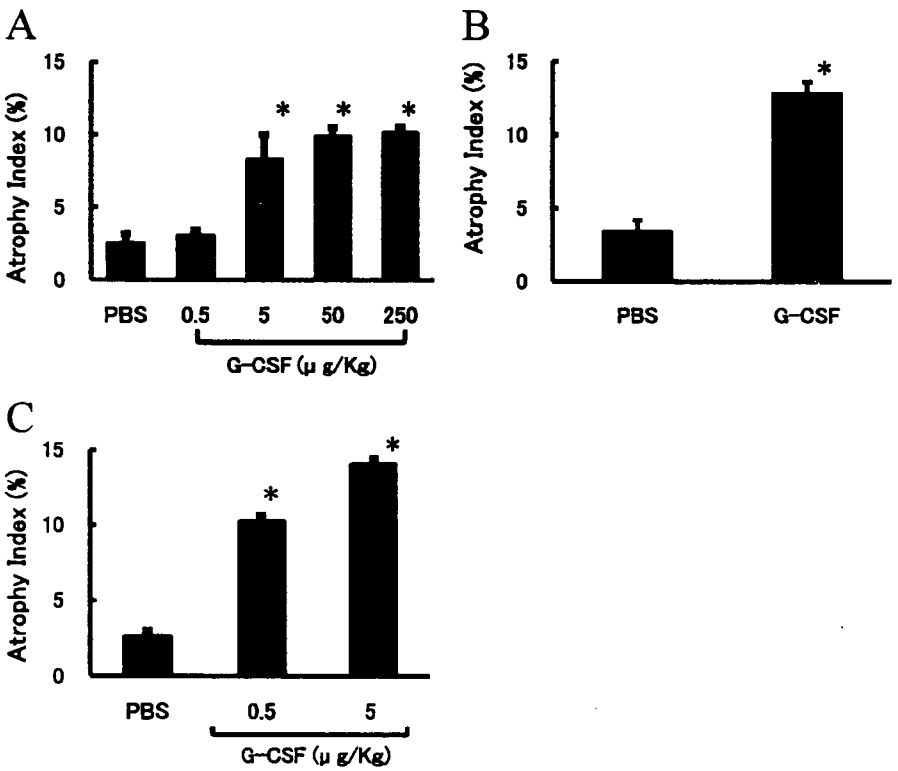

FIG. 3. Effect of granulocyte colony-stimulating factor (G-CSF) on brain atrophy. (A) G-CSF or phosphate-buffered saline (PBS) was administered 1 h after stroke and brains were evaluated grossly on day 35 post-stroke. (B) Continuous administration of G-CSF or PBS starting at 1 h post-stroke for 7 days was also tested. (C) Mouse recombinant G-CSF was administrated at the indicated dose and was found to increase the atrophy index. In each case, $n = 6$ per group. *$P < 0.05$ vs. PBS.

Discussion

Our results demonstrate that, in a murine permanent focal cerebral infarction model, administration of G-CSF, either human or murine recombinant, post-stroke is associated with enhanced brain atrophy.

In order to evaluate experimental treatments for stroke, reproducible induction of cerebral ischemia/infarction is a prerequisite. Previously, we developed a stroke model using SCID mice (Taguchi *et al.*, 2004) that proved suitable for quantification of the effect of cell therapy on neurogenesis, neovessel formation and neural function. In the current study, we have applied this stroke model to CB-17 mice and found it to provide highly reproducible data.

Granulocyte colony-stimulating factor is known to mobilize EPCs from bone marrow (Willing *et al.*, 2003) and accelerate angiogenesis (Bussolino *et al.*, 1991). Clinical studies have demonstrated that administration of G-CSF has beneficial effects in patients with acute myocardial infarction, including promotion of neovascularization and improvement of perfusion (Kuethe *et al.*, 2004). In addition, G-CSF has been shown to display neuroprotective properties in a rodent model (Schabitz *et al.*, 2003). Based on these observations, G-CSF has been tested in animal models of transient cerebral ischemia and beneficial effects have been reported (i.e. reduced infarct volume and enhanced functional recovery) (Schabitz *et al.*, 2003; Shyu *et al.*, 2004; Gibson *et al.*, 2005). In the current study, we employed a permanent cerebral infarction (i.e. stroke) model, rather than a model of transient ischemia, to investigate the effects of G-CSF.

In addition to its effects on EPCs, G-CSF is known to mobilize granuloctyes from the bone marrow, and these granulocytes have been shown to become associated with endothelia and accumulate in the ischemic brain (Justicia *et al.*, 2003). These observations suggested the possibility that G-CSF might augment the inflammatory response consequent to ischemic tissue damage by promoting recruitment and activation of neutrophils and mononuclear-derived cells (blood monocytes, monocyte-derived macrophages and microglia) (Zawadzka & Kaminska, 2005). Consistent with this concept, accumulation of CD11b-positive inflammatory cells at the border of the infarcted area was observed after treatment with G-CSF. Furthermore, a striking increase in the number of F4/80$^+$ activated macrophages/microglia was observed in non-ischemic surviving tissue (adjacent to the infarct) subsequent to administration of G-CSF. The inflammatory response after stroke has been shown to have both positive and negative effects on tissue repair (Fontaine *et al.*, 2002). Our results indicated that the balance of these inflammatory mechanisms on stroke outcome in the mouse using a permanent ischemia model and following administration of G-CSF is negative.

It would appear that the current work contradicts previous studies showing a positive effect of G-CSF after myocardial ischemia (Minatoguchi *et al.*, 2004). This apparent discrepancy may be explained, at least in part, by differences in brain and cardiac vasculature. Non-ischemic brain is protected from the systemic inflammatory response by an intact blood–brain barrier composed of endothelia joined by tight junctions. Thus, invasion of the central nervous system by activated inflammatory cells is largely prevented and the neural system functions within a relatively protected microenvironment, with respect to the inflammatory response (Neumann, 2000). However, stroke disturbs the integrity of the blood–brain barrier. We propose that a combination of impaired function of the blood–brain barrier in the context of G-CSF-induced augmentation of the inflammatory response in ischemic tissue contributes to the observed brain atrophy. Although activated inflammatory cells are known to participate in both the injurious and healing processes (Minatoguchi *et al.*, 2004), our results indicate an overall negative effect on neural function and neurogenesis following treatment with G-CSF in the post-stroke period.

In contrast to G-CSF, EPO had beneficial effects after stroke in the current model. Such positive effects are consistent with previous reports (Bernaudin *et al.*, 1999; Bahlmann *et al.*, 2004; Bartesaghi *et al.*, 2005; Kretz *et al.*, 2005) demonstrating that EPO promotes mobilization of EPCs (Bahlmann *et al.*, 2004), has angiogenic (Jaquet *et al.*, 2002) and neuroprotective properties (Bartesaghi *et al.*, 2005), and accelerates regeneration (Kretz *et al.*, 2005).

Taken together, our results indicate that administration of G-CSF after stroke results in an exaggerated inflammatory response, both at the border of the ischemic region and also in non-ischemic brain tissue, and that this is associated with brain atrophy and poor neural function. Thus, we suggest that a cautious approach should be taken in applying results of studies with G-CSF in the peripheral circulation (i.e. limb and cardiac ischemia) to the setting of cerebral ischemia. In a more general context, it is possible that agents with pro-inflammatory properties will prove less useful as therapeutic agents in cerebral ischemia in view of the above observations.

Acknowledgements

This work was partially supported by a Grant-in-Aid for Scientific Research from the Ministry of Health, Labour and Welfare. We would like to thank Y. Kasahara for technical assistance.

Abbreviations

ACA, anterior cerebral artery; EPC, endothelial progenitor cell; EPO, erythropoietin; F4/80$^+$, F4/80-positive; G-CSF, granulocyte colony-stimulating factor; MCA, middle cerebral artery; PBS, phosphate-buffered saline; SCID, severe combined immunodeficient; TTC, 2,3,5-triphenyltetrazolium.

References

Asahara, T., Murohara, T., Sullivan, A., Silver, M., van der Zee, R., Li, T., Witzenbichler, B., Schatteman, G. & Isner, J.M. (1997) Isolation of putative progenitor endothelial cells for angiogenesis. *Science*, **275**, 964–967.

Bahlmann, F.H., De Groot, K., Spandau, J.M., Landry, A.L., Hertel, B., Duckert, T., Boehm, S.M., Menne, J., Haller, H. & Fliser, D. (2004) Erythropoietin regulates endothelial progenitor cells. *Blood*, **103**, 921–926.

Bartesaghi, S., Marinovich, M., Corsini, E., Galli, C.L. & Viviani, B. (2005) Erythropoietin: a novel neuroprotective cytokine. *Neurotoxicology*, **26**, 923–928.

Bernaudin, M., Marti, H.H., Roussel, S., Divoux, D., Nouvelot, A., MacKenzie, E.T. & Petit, E. (1999) A potential role for erythropoietin in focal permanent cerebral ischemia in mice. *J. Cereb. Blood Flow Metab.*, **19**, 643–651.

Bussolino, F., Ziche, M., Wang, J.M., Alessi, D., Morbidelli, L., Cremona, O., Bosia, A., Marchisio, P.C. & Mantovani, A. (1991) In vitro and in vivo activation of endothelial cells by colony-stimulating factors. *J. Clin. Invest.*, **87**, 986–995.

Campanella, M., Sciorati, C., Tarozzo, G. & Beltramo, M. (2002) Flow cytometric analysis of inflammatory cells in ischemic rat brain. *Stroke*, **33**, 586–592.

Dzau, V.J., Gnecchi, M., Pachori, A.S., Morello, F. & Melo, L.G. (2005) Therapeutic potential of endothelial progenitor cells in cardiovascular diseases. *Hypertension*, **46**, 7–18.

Ehrenreich, H., Hasselblatt, M., Dembowski, C., Cepek, L., Lewczuk, P., Stiefel, M., Rustenbeck, H.H., Breiter, N., Jacob, S., Knerlich, F., Bohn, M., Poser, W., Ruther, E., Kochen, M., Gefeller, O., Gleiter, C., Wessel, T.C., De Ryck, M., Itri, L., Prange, H., Cerami, A., Brines, M. & Siren, A.L. (2002) Erythropoietin therapy for acute stroke is both safe and beneficial. *Mol. Med.*, **8**, 495–505.

Fontaine, V., Mohand-Said, S., Hanoteau, N., Fuchs, C., Pfizenmaier, K. & Eisel, U. (2002) Neurodegenerative and neuroprotective effects of tumor

necrosis factor (TNF) in retinal ischemia: opposite roles of TNF receptor 1 and TNF receptor 2. *J. Neurosci.*, **22**, RC216.

Gibson, C.L., Bath, P.M. & Murphy, S.P. (2005) G-CSF reduces infarct volume and improves functional outcome after transient focal cerebral ischemia in mice. *J. Cereb. Blood Flow Metab.*, **25**, 431–439.

Jaquet, K., Krause, K., Tawakol-Khodai, M., Geidel, S. & Kuck, K.H. (2002) Erythropoietin and VEGF exhibit equal angiogenic potential. *Microvasc. Res.*, **64**, 326–333.

Justicia, C., Panes, J., Sole, S., Cervera, A., Deulofeu, R., Chamorro, A. & Planas, A.M. (2003) Neutrophil infiltration increases matrix metalloproteinase-9 in the ischemic brain after occlusion/reperfusion of the middle cerebral artery in rats. *J. Cereb. Blood Flow Metab.*, **23**, 1430–1440.

Kimble, D.P. (1968) Hippocampus and internal inhibition. *Psychol. Bull.*, **70**, 285–295.

Kretz, A., Happold, C.J., Marticke, J.K. & Isenmann, S. (2005) Erythropoietin promotes regeneration of adult CNS neurons via Jak2/Stat3 and PI3K/AKT pathway activation. *Mol. Cell Neurosci.*, **29**, 569–579.

Kuethe, F., Figulla, H.R., Voth, M., Richartz, B.M., Opfermann, T., Sayer, H.G., Krack, A., Fritzenwanger, M., Hoffken, K., Gottschild, D. & Werner, G.S. (2004) Mobilization of stem cells by granulocyte colony-stimulating factor for the regeneration of myocardial tissue after myocardial infarction. *Dtsch. Med. Wochenschr.*, **129**, 424–428.

Mabuchi, T., Kitagawa, K., Ohtsuki, T., Kuwabara, K., Yagita, Y., Yanagihara, T., Hori, M. & Matsumoto, M. (2000) Contribution of microglia/macrophages to expansion of infarction and response of oligodendrocytes after focal cerebral ischemia in rats. *Stroke*, **31**, 1735–1743.

Matsushita, K., Matsuyama, T., Nishimura, H., Takaoka, T., Kuwabara, K., Tsukamoto, Y., Sugita, M. & Ogawa, S. (1998) Marked, sustained expression of a novel 150-kDa oxygen-regulated stress protein, in severely ischemic mouse neurons. *Brain Res. Mol. Brain Res.*, **60**, 98–106.

Minatoguchi, S., Takemura, G., Chen, X.H., Wang, N., Uno, Y., Koda, M., Arai, M., Misao, Y., Lu, C., Suzuki, K., Goto, K., Komada, A., Takahashi, T., Kosai, K., Fujiwara, T. & Fujiwara, H. (2004) Acceleration of the healing process and myocardial regeneration may be important as a mechanism of improvement of cardiac function and remodeling by postinfarction granulocyte colony-stimulating factor treatment. *Circulation*, **109**, 2572–2580.

Neumann, H. (2000) The immunological microenvironment in the CNS: implications on neuronal cell death and survival. *J. Neural Transm. Suppl.*, **59**, 59–68.

Schabitz, W.R., Kollmar, R., Schwaninger, M., Juettler, E., Bardutzky, J., Scholzke, M.N., Sommer, C. & Schwab, S. (2003) Neuroprotective effect of granulocyte colony-stimulating factor after focal cerebral ischemia. *Stroke*, **34**, 745–751.

Shyu, W.C., Lin, S.Z., Yang, H.I., Tzeng, Y.S., Pang, C.Y., Yen, P.S. & Li, H. (2004) Functional recovery of stroke rats induced by granulocyte colony-stimulating factor-stimulated stem cells. *Circulation*, **110**, 1847–1854.

Taguchi, A., Soma, T., Tanaka, H., Kanda, T., Nishimura, H., Yoshikawa, H., Tsukamoto, Y., Iso, H., Fujimori, Y., Stern, D.M., Naritomi, H. & Matsuyama, T. (2004) Administration of CD34+ cells after stroke enhances neurogenesis via angiogenesis in a mouse model. *J. Clin. Invest.*, **114**, 330–338.

Tamatani, M., Matsuyama, T., Yamaguchi, A., Mitsuda, N., Tsukamoto, Y., Taniguchi, M., Che, Y.H., Ozawa, K., Hori, O., Nishimura, H., Yamashita, A., Okabe, M., Yanagi, H., Stern, D.M., Ogawa, S. & Tohyama, M. (2001) ORP150 protects against hypoxia/ischemia-induced neuronal death. *Nat. Med.*, **7**, 317–323.

Walther, T., Olah, L., Harms, C., Maul, B., Bader, M., Hortnagl, H., Schultheiss, H.P. & Mies, G. (2002) Ischemic injury in experimental stroke depends on angiotensin II. *Faseb J.*, **16**, 169–176.

Wang, L., Zhang, Z., Wang, Y., Zhang, R. & Chopp, M. (2004) Treatment of stroke with erythropoietin enhances neurogenesis and angiogenesis and improves neurological function in rats. *Stroke*, **35**, 1732–1737.

Weaver, C.H., Buckner, C.D., Longin, K., Appelbaum, F.R., Rowley, S., Lilleby, K., Miser, J., Storb, R., Hansen, J.A. & Bensinger, W. (1993) Syngeneic transplantation with peripheral blood mononuclear cells collected after the administration of recombinant human granulocyte colony-stimulating factor. *Blood*, **82**, 1981–1984.

Willing, A.E., Vendrame, M., Mallery, J., Cassady, C.J., Davis, C.D., Sanchez-Ramos, J. & Sanberg, P.R. (2003) Mobilized peripheral blood cells administered intravenously produce functional recovery in stroke. *Cell Transplant.*, **12**, 449–454.

Zawadzka, M. & Kaminska, B. (2005) A novel mechanism of FK506-mediated neuroprotection: downregulation of cytokine expression in glial cells. *Glia*, **49**, 36–51.

Journal of Cerebral Blood Flow & Metabolism (2008) 28, 445–449

www.jcbfm.com

Brief Communication

Circulating CD34-positive cells provide a marker of vascular risk associated with cognitive impairment

Akihiko Taguchi[1], Tomohiro Matsuyama[2], Takayuki Nakagomi[2], Yoko Shimizu[1], Ryuzo Fukunaga[3], Yoshiaki Tatsumi[4], Hiroo Yoshikawa[4], Akie Kikuchi-Taura[5], Toshihiro Soma[5], Hiroshi Moriwaki[1], Kazuyuki Nagatsuka[1], David M Stern[6] and Hiroaki Naritomi[1]

[1]*Department of Cerebrovascular Disease, National Cardiovascular Center, Osaka, Japan;* [2]*Institute for Advanced Medical Sciences, Hyogo College of Medicine, Hyogo, Japan;* [3]*Department of Cerebrovascular Disease, Hoshigaoka Koseinenkin Hospital, Osaka, Japan;* [4]*Department of Internal Medicine, Hyogo College of Medicine, Hyogo, Japan;* [5]*Department of Hematology, Osaka Minami National Medical Center, Osaka, Japan;* [6]*Dean's Office, College of Medicine, Cincinnati University, Cincinnati, Ohio, USA*

Maintenance of uninterrupted cerebral circulation is critical for neural homeostasis. The level of circulating CD34-positive (CD34$^+$) cells has been suggested as an index of cerebrovascular health, although its relationship with cognitive function has not yet been defined. In a group of individuals with cognitive impairment, the level of circulating CD34$^+$ cells was quantified and correlated with clinical diagnoses. Compared with normal subjects, a significant decrease in circulating CD34$^+$ cells was observed in patients with vascular-type cognitive impairment, although no significant change was observed in patients with Alzheimer's-type cognitive impairment who had no evidence of cerebral ischemia. The level of cognitive impairment was inversely correlated with numbers of circulating CD34$^+$ cells in patients with vascular-type cognitive impairment, but not Alzheimer's type. We propose that the level of circulating CD34$^+$ cells provides a marker of vascular risk associated with cognitive impairment, and that differences in the pathobiology of Alzheimer's- and vascular-type cognitive impairment may be mirrored in levels of circulating CD34$^+$ cells in these patient populations.
Journal of Cerebral Blood Flow & Metabolism (2008) **28,** 445–449; doi:10.1038/sj.jcbfm.9600541; published online 8 August 2007

Keywords: antigens; CD34; cerebral circulation; cognitive impairment

Introduction

Maintaining integrity of the cerebral circulation has a critical role in neural homeostasis. Although analysis of risk factors for cerebrovascular disease has certainly provided insights into mechanisms of vascular disease, it is still difficult to predict accurately the contribution of vascular dysfunction in the long-term outcome of acute vascular insufficiency or in chronic neurodegenerative disorders. For example, in Alzheimer's disease (Casserly and Topol, 2004; Vagnucci and Li, 2003), assessment of a possible vascular component in the pathogenesis of neuronal degeneration is often ambiguous during a patient's lifetime.

Repair of the cerebral microcirculation has traditionally been assigned to ongoing replacement of damaged cerebral endothelium from outgrowth of preexisting vasculature. However, recent studies have identified circulating bone marrow-derived immature cells, including CD34-positive (CD34$^+$) cells, as contributors in maintenance of the vasculature; they have the potential to serve as a pool of endothelial progenitor cells (Asahara *et al*, 1997) and as a source of growth/angiogenesis factors (Majka *et al*, 2001). In a previous study, we have shown that circulating CD34$^+$ cells provide an index of cerebrovascular function (Taguchi *et al*, 2004*a*). We have also found that in a model of experimental cerebral ischemia, intravenous administration of CD34$^+$ cells improved neurologic function, at least in part, by restoring cerebral microcirculation in the ischemic area (Taguchi *et al*, 2004*b*).

Correspondence: Dr A Taguchi, Department of Cerebrovascular Disease, National Cardiovascular Center, 5-7-1 Fujishiro-dai, Suita, Osaka 565-8565, Japan.
E-mail: taguchi@ri.ncvc.go.jp
This work was supported by Grant-in-Aid for Scientific Research from the Ministry of Health, Labour, and Welfare.
Received 7 June 2007; revised 1 July 2007; accepted 2 July 2007; published online 8 August 2007

These results lead us to propose that circulating immature vascular progenitor cells contribute to neural homeostasis, at least in part, through their role in maintaining cerebral microvascular function. Using a recently developed method that allows precise measurement of the $CD34^+$ cell population in peripheral blood (Kikuchi-Taura *et al*, 2006), we have evaluated the level of circulating $CD34^+$ cells in patients with impaired neurologic function of diverse etiologies. Our goal has been to determine if there is relationship between levels of $CD34^+$ cells, impaired neural function, and vascular integrity.

Materials and methods

This study was approved by Institutional Review Boards of the respective institutions (National Cardiovascular Center, Hyogo College of Medicine, Hoshigaoka Koseinenkin Hospital, and Osaka Minami National Medical Center). All subjects provided informed consent. Individuals with Mini Mental State Examination Score (MMSE) <24 and Clinical Dementia Rating (CDR) ≥ 0.5 were enrolled in this study and defined as having impaired cognitive function. In the view of history, evaluation of symptoms, and results of brain imaging studies (magnetic resonance imaging and single photon-computed tomography), patients with cognitive impairment were divided into two groups by neurologists blinded to the experimental protocol: vascular-type cognitive impairment or Alzheimer's-type cognitive impairment, according to the criteria of *Diagnostic and Statistical Manual of Mental Disorders* (4th ed, DSM-4) (American Psychiatric Association, 1994). To exclude the contribution of vascular element in patients with Alzheimer's-type cognitive impairment, patients' coexistent Alzheimer's-type cognitive impairment and cerebral infarction, observed by magnetic resonance imaging, were excluded from this study. In addition, patients with cognitive impairment diagnosed as neither of the Alzheimer's type nor vascular type were excluded. A total of 95 individuals, including 32 age-matched control subjects with no history of vascular disease, no neuronal deficiency, and no cognitive impairment, were enrolled. In addition, individuals excluded from the study included: premenopausal women, patients who experienced a vascular event within 30 days of measurements, history of cerebral hemorrhage, and evidence of infection or malignant disease. Using a modification of the International Society of Hematotherapy and Graft Engineering (ISHAGE) Guidelines (Sutherland *et al*, 1996), the number of circulating $CD34^+$ cells was quantified as described (Kikuchi-Taura *et al*, 2006). In brief, blood samples were incubated with phycoerythrin-labeled anti-CD34 antibody, fluorescein isothiocyanate-labeled anti-CD45 antibody, 7-aminoactinomycin-D, and internal control (all of these reagents are from the Stem-Kit, Beckman Coulter, Marseille, France). 7-Aminoactinomycin-D-positive dead cells and CD45-negative cells were excluded, and the number of cells forming a cluster with characteristic $CD34^+$ cells (i.e., low side scatter and low-to-intermediate CD45 staining) was counted. The absolute number of $CD34^+$ cells was calculated using the internal control. In this study, we used a single measurement at the time of entry into the study, on the basis of our previous observation that the level of circulating $CD34^+$ cells is relatively stable (Taguchi *et al*, 2004*a*). For statistical analysis, JMP version 5.1J (SAS Institute Inc, Co, NC, USA) was used. Individual comparisons were performed using a two-tailed, unpaired Students' *t*-test. Statistical comparisons among groups were determined using analysis of variance. Mean $\pm$ s.e. is shown.

Results

Baseline characteristics of the groups are shown in Table 1. In univariate analysis of control subjects, each cerebrovascular risk factor and other treatment showed no significant difference with the number of circulating $CD34^+$ cells (data not shown).

To investigate a possible relationship between circulating $CD34^+$ cells and cognition, the level of circulating $CD34^+$ cells was compared among these groups. Representative fluorescence-activated cell sorting images are shown in Figure 1A (vascular-type) and 1B (Alzheimer's-type). Analysis of variance revealed a significant decrease of $CD34^+$ cells in patients with vascular-type cognitive impairment compared with Alzheimer's-type cognitive impairment ($P<0.001$) and normal subjects ($P<0.001$, Figure 1C).

To investigate further a possible association of circulating $CD34^+$ cells with cognitive impairment, patients with vascular-type impaired cognition were divided into two groups according to their CDR (mild: CDR $=0.5$, $n=22$, mean age $=75.2\pm1.6$ years; moderate-severe: CDR ≥ 1, $n=18$, mean age $=75.3\pm1.5$ years) or MMSE (mild: MMSE ≥ 20, $n=25$, mean age $=74.2\pm1.4$ years; moderate-severe: MMSE <20, $n=15$, mean age $=77.1\pm1.5$ years). The results showed a significant decrease in the level of circulating $CD34^+$ cells in moderate-severe group, based on stratification by either CDR (Figure 1D, $P=0.01$) or MMSE (Figure 1E, $P=0.03$) in patients with vascular-type cognitive impairment. Similar analysis was applied to patients with Alzheimer's-type impaired cognition. They were divided into two groups according to CDR (mild: $n=8$, mean age $=73.0\pm4.7$ years; moderate-severe: $n=15$, mean age $=77.5\pm1.9$ years) or MMSE (mild: $n=12$, mean age $=74.1\pm3.0$ years; moderate-severe: $n=11$, mean age $=77.8\pm2.9$ years). However, in contrast to patients with vascular-type impaired cognition, there was no significant difference observed in patients with Alzheimer's-type cognitive impaired, based on CDR (Figure 1F, $P=0.86$) or MMSE (Figure 1G, $P=0.60$).

Discussion

Our results are consistent with a contribution of circulating $CD34^+$ cells in support of cognitive function, presumably through their positive homeostatic influence on the cerebral circulation in

Table 1 Baseline characteristics

	Total	Cognitive impairment		Control	P-value for trend
		Vascular-type	Alzheimer's-type		
n	95	40	23	32	
Age, years	74.9±0.6	75.3±1.1	75.9±2.1	74.2±0.7	0.53
Male gender, *n* (%)	57 (60)	27 (68)	12 (52)	18 (56)	0.46
Risk factor, n (%)					
Hypertension	41 (43)	21 (53)	9 (39)	11 (34)	0.28
Hyperlipidemia	29 (31)	14 (35)	5 (22)	10 (31)	0.53
Diabetes mellitus	9 (9)	5 (13)	1 (4)	3 (9)	0.57
Smoking	20 (21)	10 (25)	6(26)	4 (13)	0.34
Treatment, n (%)					
Ca-channel blocker	30 (32)	15 (38)	6 (26)	9 (28)	0.56
β-Blocker	2 (2)	1 (3)	0 (0)	1 (3)	0.71
ACE inhibitor	4 (4)	3 (8)	1 (4)	0 (0)	0.29
ARB	8 (8)	3 (8)	3 (13)	2 (6)	0.65
Diuretics	6 (6)	2 (5)	1 (4)	3(9)	0.68
Statin	29 (31)	14 (35)	5 (22)	10 (31)	0.54
Aspirin	28 (29)	23 (58)	1 (4)	4 (13)	<0.01
Ticlopidine	11(12)	9 (23)	0 (0)	2 (6)	0.01

ACE, angiotensin-converting enzyme; ARB, angiotensin II receptor blocker.

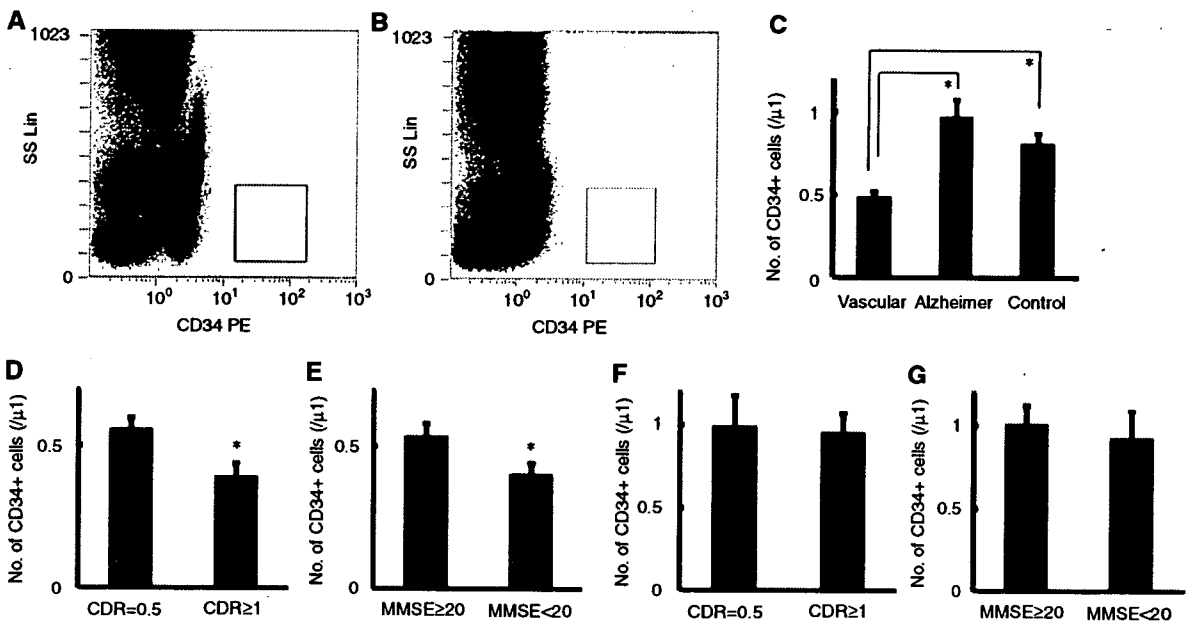

Figure 1 Levels of circulating CD34+ cells and cognitive impairment. (**A** and **B**) After exclusion of 7-AAD-positive dead cells and CD45-negative cells (non-leukocyte), CD34+ cells cluster at low side scatter were clearly observed (**A**, vascular-type; **B**, Alzheimer's-type). (**C**) Analysis of variance revealed a significant decrease in circulating CD34+ cells in patients with vascular-type cognitive impairment compared with normal subjects and individuals with Alzheimer's-type cognitive impairment. In contrast, no significant change in circulating CD34+ cells was observed in patients with Alzheimer's-type cognitive impairment compared with control subjects. (**D** and **E**) In the group of patients with vascular-type cognitive impairment, the level of circulating CD34+ cells was significantly reduced in patients with more severe cognitive impairment compared with the more mildly affected group (**D**, CDR; **E**, MMSE). (**F** and **G**) In contrast, no significant difference was observed in patients with Alzheimer's-type cognitive impairment based on assessment of cognition (**F**, CDR; **G**, MMSE). SS Lin, side-scatter linear scale. $^*P < 0.05$.

settings of ischemic stress. Further, these observations suggest a basic difference between the pathobiology of dementia in Alzheimer's disease (without associated cerebral ischemia) and declining cognitive function in patients with ischemic cerebrovascular disorders.